Experimental Investigation of Unsteady Tornadic Wind Loads on Structures

Prepared by M. C. Jischke, F. Moslehi

School of Aerospace, Mechanical & Nuclear Engineering
University of Oklahoma

NOTICE

Availability of Reference Materials Cited in NRC Publications

Most documents cited in NRC publications will be available from one of the following sources:

1. The NRC Public Document Room, 1717 H Street, N.W.
   Washington, DC 20555

2. The NRC/GPO Sales Program, U.S. Nuclear Regulatory Commission,
   Washington, DC 20555

3. The National Technical Information Service, Springfield, VA 22161

Although the listing that follows represents the majority of documents cited in NRC publications, it is not intended to be exhaustive.

Referenced documents available for inspection and copying for a fee from the NRC Public Document Room include NRC correspondence and internal NRC memoranda; NRC Office of Inspection and Enforcement bulletins, circulars, information notices, inspection and investigation notices; Licensee Event Reports; vendor reports and correspondence; Commission papers; and applicant and licensee documents and correspondence.

The following documents in the NUREG series are available for purchase from the NRC/GPO Sales Program: formal NRC staff and contractor reports, NRC-sponsored conference proceedings, and NRC booklets and brochures. Also available are Regulatory Guides, NRC regulations in the *Code of Federal Regulations*, and *Nuclear Regulatory Commission Issuances.*

Documents available from the National Technical Information Service include NUREG series reports and technical reports prepared by other federal agencies and reports prepared by the Atomic Energy Commission, forerunner agency to the Nuclear Regulatory Commission.

Documents available from public and special technical libraries include all open literature items, such as books, journal and periodical articles, and transactions. *Federal Register* notices, federal and state legislation, and congressional reports can usually be obtained from these libraries.

Documents such as theses, dissertations, foreign reports and translations, and non-NRC conference proceedings are available for purchase from the organization sponsoring the publication cited.

Single copies of NRC draft reports are available free, to the extent of supply, upon written request to the Division of Technical Information and Document Control, U.S. Nuclear Regulatory Commission, Washington, DC 20555.

Copies of industry codes and standards used in a substantive manner in the NRC regulatory process are maintained at the NRC Library, 7920 Norfolk Avenue, Bethesda, Maryland, and are available there for reference use by the public. Codes and standards are usually copyrighted and may be purchased from the originating organization or, if they are American National Standards, from the American National Standards Institute, 1430 Broadway, New York, NY 10018.

GPO Printed copy price: $4.50

Experimental Investigation of Unsteady Tornadic Wind Loads on Structures

Prepared by
M. C. Jischke, F. Moslehi

School of Aerospace, Mechanical & Nuclear Engineering
University of Oklahoma
865 Asp Avenue
Norman, OK 73069

PREFACE

This investigation was sponsored by the United States Nuclear
Regulatory Commission under Contract No. NRC-04-78-207. This work was
conducted by Professor Martin C. Jischke and Farid Moslehi; School of
Aerospace, Mechanical and Nuclear Engineering, University of Oklahoma;
Norman, Oklahoma 73019. Mr. Kellogg V. Morton, NRC, served as the
contracting officer.

This report is taken, in part, from the thesis of Farid Moslehi, "On
the Dynamic Interaction of a Tornado-like Vortex with Structures",
submitted to the University of Oklahoma.
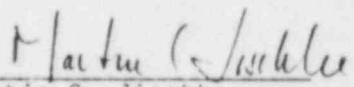
Martin C. Jischke
Principal Investigator
April 24, 1984

ABSTRACT

Ward's tornado simulator was used to model the effects of a tornado-like vortex on a cylindrical model structure. The cylindrical model, intended to represent a containment building of a nuclear reactor, is a circular cylinder 17 cm in height and 11.4 cm in diameter with a hemispherical roof. The experiment was conducted at swirl angles of 0° and 45°. Pressure coefficients were measured at different locations on the model for steady and unsteady cases, corresponding to situations where the relative velocity between the vortex and model is zero and nonzero.

Results are presented in the forms of sectional pressure coefficient profiles, and sectional force coefficients. Pressure profiles show that there are significant differences between the steady and unsteady results. Translation of the model through the simulator produces a more symmetric pressure distribution, and also results in a more substantial pressure drop on the model.

It is observed that in a flow with swirl angle of 45°, translation causes a significant increase in the horizontal sectional force coefficient. Outside of the core region, translation causes an increase in the axial sectional force coefficient. The formation of very low pressure regions over the top section of the structure leads to very strong axial force coefficients. This may cause the failure to first appear on the roof, and then propagate throughout the structure and cause total failure.

TABLE OF CONTENTS

TABLE OF CONTENTS (cont'd)

LIST OF FIGURES

LIST OF PLATES

NOMENCLATURE

(and some typical values)

a   cylinder radius (5.7 cm)

C_D drag coefficient

$\vec{C}_F$ force coefficient

D   cylinder diameter (11.4 cm)

$\vec{F}$ force

h   depth of the inflow layer (50.4 cm)

L   length scale

q   volumetric flow rate per unit area

Q   volumetric flow rate

r,θ,z polar coordinates

r_c core radius   (~ 10 cm)

r_u updraft radius   (~ 58 cm)

R   total force per unit length

S   swirl ratio (0.4)

t   time

u,v,w   polar cylindrical components of velocity

u_{ref} reference velocity, based on the average radial velocity between the screen and the core radius (~ 100 cm/s)

u_s radial components of velocity at the screen

v_s azimuthal component of velocity at the screen

x

V_{ref} reference velocity, based on the velocity at core radius (~ 600 cm/s)

v_{tr} translational velocity (61 cm/s)

$\vec{V}$ velocity vector

V_o magnitude of the velocity due to the vortex-sink combination

w axial component of velocity

W complex potential

x,y,z Cartesian coordinates

z_r surface roughness height (0.2 cm)

Z complex variable

α inverse of exponent in power law variation of velocity with height (~ 3 to 7)

Γ circulation

μ dynamic viscosity ($1.7 \times 10^{-4} \frac{g}{cm \, s}$)

$\vec{\omega}$ vorticity

Φ velocity potential

ϕ imposed swirl angle ($0°$, $45°$)

Ψ stream function

ρ density (0.0012 g/cm^3)

τ_c vorticity convection time scale

τ_p vorticity production time scale

ξ, η, ζ polar cylindrical components of vorticity

CHAPTER I

INTRODUCTION

1.1 Motivation

The field of wind engineering has been receiving growing attention. New ideas in design, incorporation of new materials, and a growing awareness in the areas of efficiency, safety, and environmental impact have all contributed to rapid development of wind engineering. These factors play an even greater role when we consider the design of vital structures. A nuclear power plant is an example of such a structure. Nuclear power plant housings are among the most challenging problems of structural design. Safety requirements of a nuclear power plant require very sophisticated designs. In addition to other demanding requirements, a nuclear power plant must be able to withstand wind loads as well as the impact of wind generated missiles. As the construction costs of these structures are almost prohibitively expensive, such structures cannot be grossly over-designed. Therefore, safety and economic considerations require a very thorough and careful analysis of all aspects of design. The effects of wind on structures is still a developing field with many interesting, as well as unsolved, problems. Aside from the reasons given so far, the richness and complexity of wind engineering problems generates a great deal of interest in engineering enthusiasts.

1

1.2 Preliminary Remarks

In the past, much of the attention has been focused on the inter-action of boundary layer-type winds with structures. Although the problem is far from being completely solved, much progress has been made in this area. Numerous laboratory experiments and field observations have led to construction codes and regulatory measures. However, the most severe wind conditions encountered in nature are not boundary layer-type winds. An examination of different wind conditions, and order-of-magnitude estimates, lead to the conclusion that the most severe wind conditions are associated with tornadoes (1). Tornadic wind speeds of close to 400 kph have been reported (2). Tornadic flows are very different from boundary layer winds. Boundary layer-type winds, generally, contain only horizontal vorticity. Tornadic flows contain both horizontal and vertical (axial) vorticity. In fact, being fully three-dimensional, unsteady, turbulent, and vortical, tornadic flows are among the richest and most complex problems of fluid dynamics. Aerodynamic effects of a tornadic flow on a structure are believed to be very different than those associated with boundary layer-winds.

There are three different approaches to the study of the tornado-structure interaction problem: analytical, computational, and experimental. As it was mentioned earlier, the physics of the flow is so complex that a detailed analytical approach based on fundamentals of fluid dynamics is very difficult. As we shall see in subsequent sections, even the relatively simple formulations of the problem, lead to highly nonlinear interaction problems. Complicated nonlinear

2

problems of this nature often do not lend themselves to successful computer modelling and simulation. In addition, the computer requirements in terms of time and cost are still prohibitively expensive. Therefore, one is left with the experimental alternative.

The unpredictable and very dangerous nature of tornadoes, does not allow for actual field measurements. However, given that one has enough insight into the problem, the flow may be reproduced and studied in a laboratory. Furthermore, laboratory simulation allows for the study of a wide range of tornado-like flows and their effects on different structures.

1.3 Literature Survey

In spite of the importance of the tornadic interaction problem, little is known about this phenomenon. The main thrust of wind engineering research has been directed towards the boundary layer-type winds and their effects on structures. Davenport (3), Jensen and Frank (4,5), Cermak (6), Marshall and Thom (7), and Parmelee (8) have studied the interaction of steady boundary layer winds with structures. The experimental study of the tornadic interaction with structures is limited to the experiments of Chang (9), and Jischke & Light (10). In addition to these experiments, there have been attempts to study the problem by observing tornado-damaged structures. In this approach, one attempts to arrive at the cause, given the effect. Mehta, Minor, and McDonald (11), and McDonald (12) analyze the damage, and suggest probable wind speeds required to have caused the damage. This type of analysis has many limitations. It requires an a priori knowledge of the

3

structural integrity and assumptions regarding failure mechanisms. In
addition, determining the damage sequence itself may prove to be a for-
midable task. The uncertainties in this type of analysis make the re-
sults unsuitable for important applications, such as the design of
vital structures. Therefore, it is concluded that laboratory simula-
tions are likely to produce the most useful results.

In the experimental measurements of Chang (9), a cubical model was
rotated about the axis of a vortex. The vortex flow was produced in a
tornado simulator. The parameters were chosen such that the small cube
was to represent an average house. Chang's experiments may be criti-
cized as a genuine "dynamic" simulation, because the relative distance
between the vortex and the structure is not varied. A more complete
simulation of the tornadic interaction must account for the unsteady
features associated with the tornado approaching toward and then recod-
ing from a structure.

Another simulation study of the interaction problem is due to
Jischke & Light (10). This study is only concerned with the steady
effects, and ignores all unsteady features.

The unsteady effects associated with the translation of a tornado
remain to be studied, and require further investigation.

1.4 Definition of the Problem

Our goal is to investigate the unsteady effects due to the
relative motion of a model structure and a tornado-like vortex flow.
In order to isolate the unsteady effects, one must study both the

4

steady and unsteady phenomena. Then, by comparison, it becomes possible to understand the significance of the unsteady effects. Here, by the term "effects", we ultimately mean the forces and the distribution of pressure on the structure.

CHAPTER II

LABORATORY SIMULATION OF TORNADOES AND THEIR

INTERACTION WITH STRUCTURES

2.1 Natural Tornadoes

A thorough understanding of tornadoes, as they naturally

occur, is essential to successful laboratory simulation. As described

by Kessler (13): ". . . The tornado is identified by a rapidly rotat-

ing funnel-shaped cloud that marks the condensation boundary of in-

spiraling air at low altitudes that undergoes adiabatic expansion and

cooling. Usually the funnel is on the southwest side of the major

thunderstorm. The funnel cloud extension toward the ground increases

with lowering pressure in the core and higher ambient humidity."

Tornadoes are among the most destructive natural disasters.

Annually they claim many lives, and cause hundreds of millions of

dollars in property damage. The occurence of tornadoes is highly un-

predictable. Associated with tornadoes are the most destructive winds

and extremely rapid changes in the atmospheric pressure. Tornadoes are

capable of blowing over, exploding or bursting (due to the difference

between the inside and outside pressures), and literally lifting struc-

tures.

The life cycle of a tornado may be divided into three distinct

6

stages: genesis, mature stage, and decay. Little is known about the physical processes involved during the genesis and decay stages of a tornado. However, these two stages are not as important as the mature stage in the interaction problem. Maximum wind speeds and most of the destruction occur during the mature stage. In most cases, a tornado does not remain in its mature stage for more than a few minutes. During this period, rotational speeds could easily exceed 100 m/s, and the flow becomes compressible. At the same time, the translational speeds may be about 10 m/s to 30 m/s. Figure (1) provides a sketch of a tornado during its mature stage. The basic mechanism is the low level convergence of rotating ambient air through the so-called surface inflow layer. The convergence is induced by the upward motion of air through the updraft region. As the flow converges radially, it rotates faster to conserve angular momentum. In the close vicinity of the axis of rotation, velocity gradients become very large. Viscous effects eventually dominate, and produce a region of rigid rotation. This region is known as the core region of the flow.

2.2 Kinematics of the Flow

The simplest and most widely used model to describe the mature stage is a combined Rankine vortex. The flow is divided into two regions. The core region which is described as a solid body rotation region. Outside of the core, the flow is described by a potential vortex. Therefore, the vorticity is assumed to be zero everywhere outside the core. At the critical radius, the edge of the core region, vorticity undergoes a finite jump. In other words, the combined Rankine vortex

7
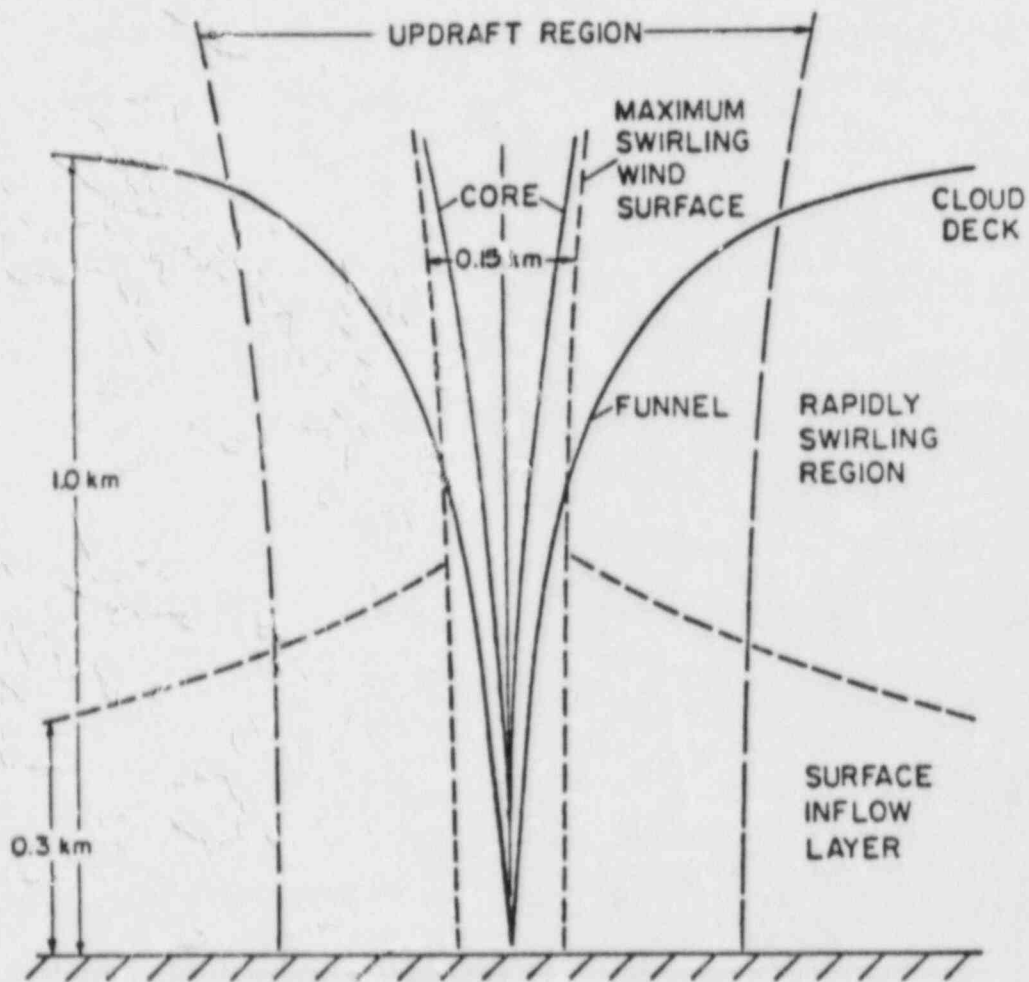
Figure 1. The lower 1 km of a mature stage tornado.

assumes that all of the vorticity is concentrated along the axis of rotation, within the core region.

If one accepts the combined Rankine vortex as an adequate model, then the flow in the convergence zone may be explainable by the potential flow theory. We will return to this discussion in subsequent sections to evaluate the potential flow model, as well as some other alternatives.

The information about the velocity distribution in naturally occurring tornadoes is rather limited. The velocity distribution data for the 1957 Dallas tornado were reported by Hoecker (14,15). This data was based on the available motion pictures of this tornado. Another source is the motion picture analysis of the 1963 Kankakee tornado by Goldman (16). Although the method incorporates some arbitrariness, it is the only direct approach which has yielded reasonable results. Hoecker's data are given in Figure 2.

2.3 Laboratory Simulation of Tornadoes

In the study of the tornadic interaction problem, one is primarily concerned with the lower 1 km of the flow field. A source of rotation and a sink are required to produce a tornado-like flow in the laboratory. It is important to be able to control these two sources independently. The inflow layer through which the flow converges must be restricted to low-levels. Low-level convergence appears to be an essential requirement for the concentration of vorticity into a tornado-like vortex. An important feature of a tornado is the additional core pressure deficit which is due to dry-adiabatic descent along the axis

9
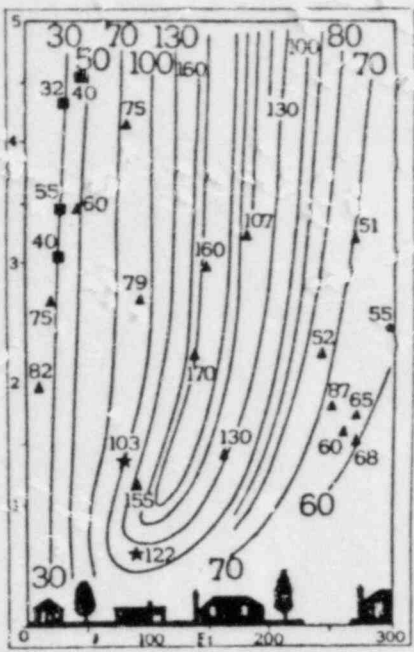
radial velocity
(MPH)
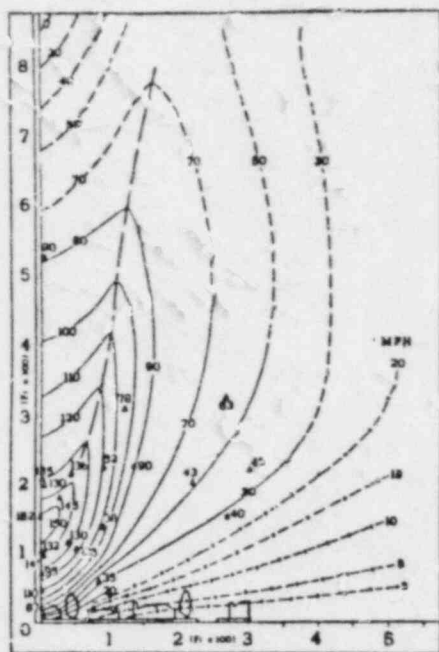
axial velocity
(MPH)

motion picture analysis of:

★ ▲ Solid Debris Particles
● Cloud and Dust Parcels
■ Funnel Surface

Figure 2. Velocity distribution along the radius and height of a
tornado (Hoecker, 14).

of the vortex. The additional core pressure deficit is believed to be responsible for the formation of multi-celled vortices.

A number of tornado simulators have been designed and built to this date. A survey of some of the more important designs can be found in a report by Monji (17). One of the most successful designs is due to Ward (18). Ward's tornado simulator is capable of reproducing most of the essential features of tornadoes. Spectacular features such as "vortex breakdown" and "core-splitting" have been simulated in Ward's tornado simulator. There are striking similarities between the velocity profiles in the Ward simulator and those reported by Hoecker. The surface pressure profile in the simulator and available data from the Newton, Kansas tornado (19) exhibit remarkable similarities also.

Jischke and Parang (20,21) conducted a thorough investigation of the flow in the Ward simulator. Their studies confirmed the fact that this simulator is in fact capable of accurately reproducing tornado-like flows.

Figure 3 shows a schematic sketch of the Ward tornado simulator. Generally speaking, Ward's simulator is a right circular cylinder with a mesh wire (screen) section. The screen may be rotated independently, and at a variety of angular velocities. A variable speed exhaust fan on the top section of the cylinder draws the air through the screen and inside the cylinder. Thus, air is given an inward radial velocity, and as it passes through the screen, it is given angular momentum by the screen. A honeycomb baffle is used to decouple the fan induced rotation from the rotation caused by the screen. This layer of honey-comb baffle is believed to be responsible for simulating the core

11
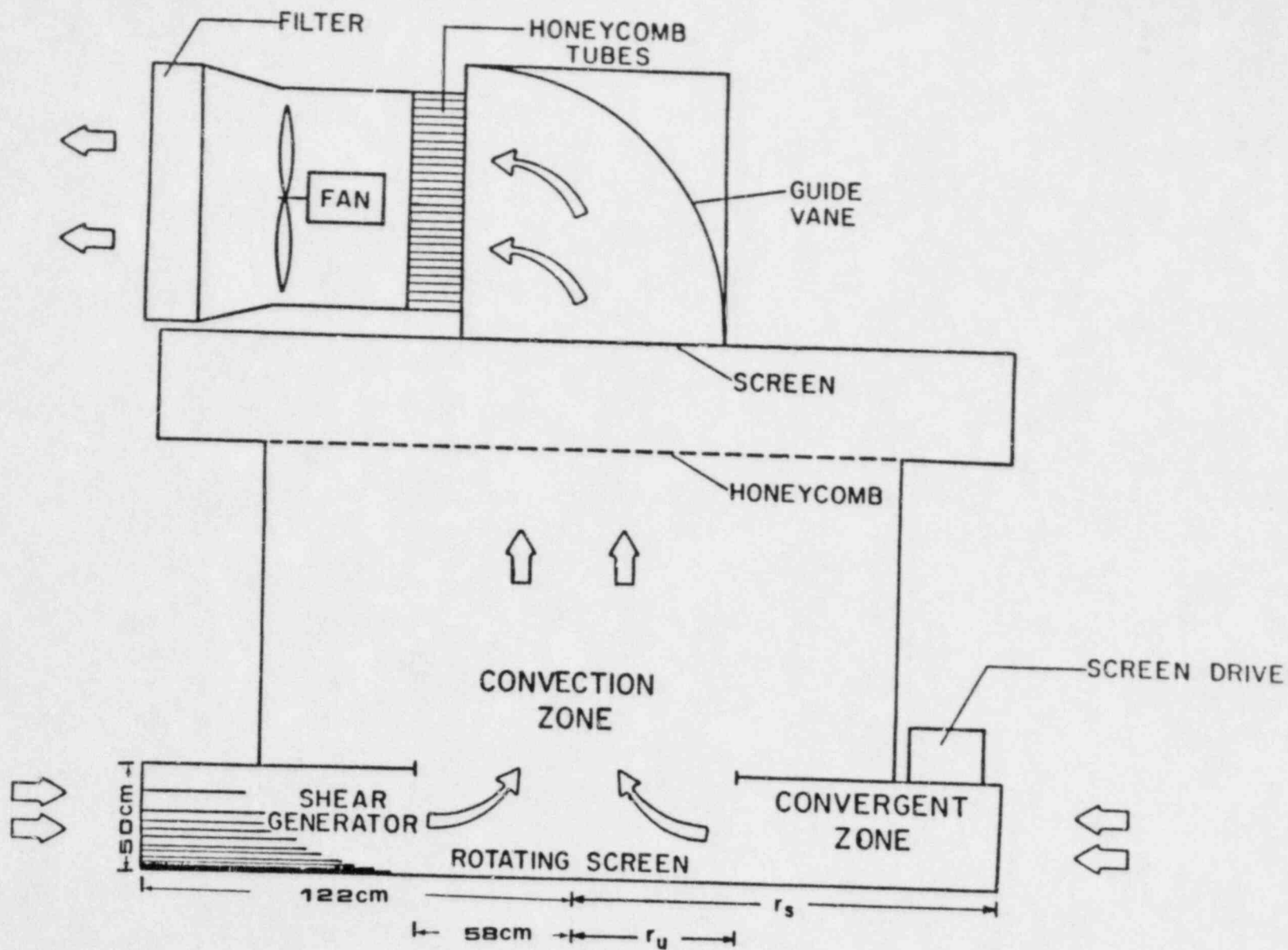
Figure 3. Ward Tornado Simulator

pressure deficit which was discussed earlier. The geometric features of the vortex are controlled by the updraft radius and the height of the inflow-layer.

Added features, which were not included in the original design, include variable porosity screen and surface roughness. Variable porosity screen is used to simulate the far field boundary layer. Surface roughness simulates the topographical features, and also, maintains the turbulent character of the flow.

2.4 Scaling Analysis

To meaningfully simulate the dynamic interaction phenomenon, dynamic similarity must be attained. Let us first examine the important physical parameters. These parameters are:

Q volumetric flow rate

Γ far field axial circulation

ν kinematic viscosity

h height of the inflow layer

r_u updraft radius

r_c core radius

The important dimensionless parameters characterizing the flow are:

$\dfrac{h}{r_u}$ aspect ratio

$\dfrac{r_c}{r_u}$ configuration ratio

$\dfrac{\Gamma r_u}{2Q}$ swirl ratio

$\dfrac{\Gamma}{\nu}$ radial Reynolds number

13

Davies-Jones (24), and Jischke and Parang (21) showed the configuration ratio is a function of swirl ratio only. Therefore, the flow is characterized by three dimensionless parameters: aspect ratio, swirl ratio, and Reynolds number. Aspect ratio determines the geometry of the flow. Swirl ratio is the kinematic similarity parameter, and Reynolds number is needed for dynamic similarity.

It is possible to express the swirl ratio in a different representation. Consider the flow as it crosses the screen and enters the simulator. Then, volumetric flow rate and circulation at the screen may be written as:

$$Q_S = 2\pi \, r_S h \, u_S \tag{1}$$

$$\Gamma_S = 2\pi \, r_S \, v_S \tag{2}$$

u_S and v_S are the radial and tangential components of velocity, respectively. In terms of u_S and v_S we obtain the following expression for the swirl ratio:

$$S = \frac{\left(\dfrac{v_S}{u_S}\right)}{2\left(\dfrac{h}{r_u}\right)} \tag{3}$$

The inflow angle at the screen ϕ, is defined by the relationship,

$$\tan \phi = \frac{v_S}{u_S} \tag{4}$$

Therefore, swirl ratio becomes

$$S = \frac{\tan \phi}{2(\text{Aspect Ratio})} \tag{5}$$

Equation (5) has far reaching practical implications. It is much easier to measure ϕ than it is to measure Γ.

A more accurate model of the flow requires the simulation of the far-field boundary layer, and the addition of surface roughness. By

14

varying the porosity of the screen, it is possible to shear the velocity profile such that it resembles the typical velocity profile of atmospheric winds. At relatively close distances to the ground, the wind velocity is assumed to obey a power-law variation. Therefore, we may write

$$\frac{V}{V_0} = \left(\frac{z}{z_0}\right)^{1/\alpha} \tag{6}$$

V_0 is the wind velocity at height z_0. α is a constant and is determined experimentally. According to the experimental results, given by Cermak (25), α has a range of values between 3 and 7. A variable porosity screen is used in the present study to produce such a velocity profile at the screen. The porosity is varied by placing strips of tape (drag elements) on the screen. A discussion of this technique is given by Cockrell and Lee (26). Such a boundary layer achieves equilibrium within a few drag element diameters if the flow is non-accelerating. However, in a tornado simulator, there is a radial pressure gradient which accelerates the flow. The equilibrium of the sheared velocity profile was not studied at the time of the experiment. The surface roughness was added for two reasons. First, the roughness elements are needed to simulate the topographical features. Secondly, surface roughness maintains the turbulent character of the flow. The important parameter associated with surface roughness is the ratio of the typical roughness element to the core radius, $\frac{z_r}{r_c}$.

The effects of a sheared velocity profile, and surface roughness are discussed by Light (27), and Leslie (28), respectively. Leslie

15

(28) studied the effects of the Reynolds number on the flow, and concluded that the flow has a very weak dependence on the Reynolds number. Therefore, it is possible to establish dynamic similarity without necessarily matching the Reynolds number. This is done by adjusting the velocity profile, surface roughness, and swirl ratio. The importance of this idea is realized when one considers the great difficulties of producing Reynolds numbers of the order of 10^9 in the laboratory.

The characteristic length scale of the structure, L, and the core radius, r_c, are used to form the dimensionless parameter $\frac{L}{r_c}$. This parameter determines the size of the model structure. An additional similarity parameter arises when we consider the kinematics of tornado translation. To establish a similarity parameter associated with the translational effects, let us consider the Bernoulli equation and assume $\frac{\partial \phi}{\partial t}$ is small compared to the dynamic pressure:

$$\frac{P_{\infty \text{unsteady}}}{P_{\infty \text{steady}}} = \frac{\frac{1}{2} \rho (V_{ref} + V_{tr})^2}{\frac{1}{2} \rho V_{ref}^2}$$

$$= \left(1 + \frac{V_{tr}}{V_{ref}}\right)^2$$

Since $\frac{V_{tr}}{V_{ref}}$ is a small parameter, then

$$\frac{P_{\infty \text{unsteady}}}{P_{\infty \text{steady}}} = 1 + 2 \frac{V_{tr}}{V_{ref}}$$

Therefore, the important translation parameter is $\frac{V_{tr}}{V_{ref}}$ where V_{tr} is the translation velocity of the vortex, and V_{ref} is a reference velocity, such as the maximum radial velocity which occurs at the edge of the core. The motion of the vortex, in the Ward apparatus, poses great difficulties. Therefore, it was decided to move the model relative to the steady vortex. Although these two cases are not identical, we

16

assume that the important features for both cases are the same. Further discussions on this matter are provided in the subsequent sections, where we explore the mathematical description of the flow.

Table 1 shows the important parameters as they occur naturally, an their counterparts in laboratory simulation.

2.5 Experimental Apparatus

A cylindrical model with a hemispherical roof was constructed to model a typical nuclear reactor containment building. Ward simulator was modified such that it was possible to move this model along the floor section. The translation mechanism (track) is capable of carrying both the model and pressure measuring devices. A detailed description of the track is given by Light (27). Figure 4 shows a sketch of the track. The important property of the flow for our purposes is the distribution of pressure on the model. Pressure was measured at different locations on the surface of the model as it moved through the simulator. In addition to the pressure, displacement, velocity and acceleration of the model were also monitored and r orded. Therefore, it was possible to construct the pressure distribution on the model as it moved through the vortex. A number of pressure ports were drilled through the model. These holes were connected to a pressure transducer, one at a time. The signal was routed to a null-offset adapter, where it was offset by an amount equal to the atmospheric pressure. Therefore, the signal leaving the null-offset adapter was the difference between the pressure on the model and the atmospheric pressure. The signal was then sent to an electronic manometer. The output signal

Dimensionless Parameter	Hoecker's Data	Ward Simulator
Aspect ratio, $\dfrac{h}{r_u}$	1.2	1.2
Swirl ratio, $\dfrac{\Gamma r_u}{2Q}$	0.4	0.4
Radial Reynolds number, $\dfrac{\Gamma}{\nu}$	$\sim 10^9$	$\sim 10^4$
Roughness parameter, $\dfrac{r_r}{r_c}$	0.02 - 0.5	~ 0.02
Velocity profile, shape parameter, α	3 - 7	4
Translation parameter, $\dfrac{V_{tr}}{V_{ref}}$	0.1 - 0.3	0.25

TABLE 1. The important dimensionless parameters associated with the tornadic interaction problem.

was further amplified, and then, it was sent to a recorder. Finally, it was recorded on photographic paper. As the pressure signal was being recorded, the displacement of the model was measured by a potentiometer. The signal from the potentiometer was electronically differentiated twice with respect to time. The first derivative is the velocity signal, and the second derivative represents the acceleration of the model. Signals corresponding to displacement, velocity, and acceleration were sent to the recorder. The recorder, simultaneously, recorded four signals corresponding to pressure, displacement, velocity, and acceleration. Figures 5a and 5b provide a schematic diagram of the instrumentation and a typical output. The response time of the system was measured experimentally to insure that no significant time lag was present in the pressure signal. An experiment was designed and carried out to measure the response time of the pressure-measuring system. The experimental apparatus consists of a sealed cylindrical chamber with a pressure tap positioned in the center at one end, and a flexible rubber diaphragm covering the opposite end. A 0-5000 rpm variable speed motor is connected to the diaphragm by a rod. As the motor turns, the diaphragm is displaced laterally which causes the pressure inside the chamber to change. By adjusting the speed of the motor, one can control the frequency at which the pressure is changed inside the chamber. A slotted hub is attached to the motor shaft, and the hub is situated along the path of an infrared light source to act as a breaker switch. The signal from the light source is sent to a dual trace oscilloscope, with a camera. Thus, as the shaft rotates, a series of sharp spikes are observed on the scope. The pressure output

19

MAIN SURFACE

LINEAR BEARING

MAIN SURFACE SLOT

20

MOTORIZED
PULLEY AND WIRE
SYSTEM

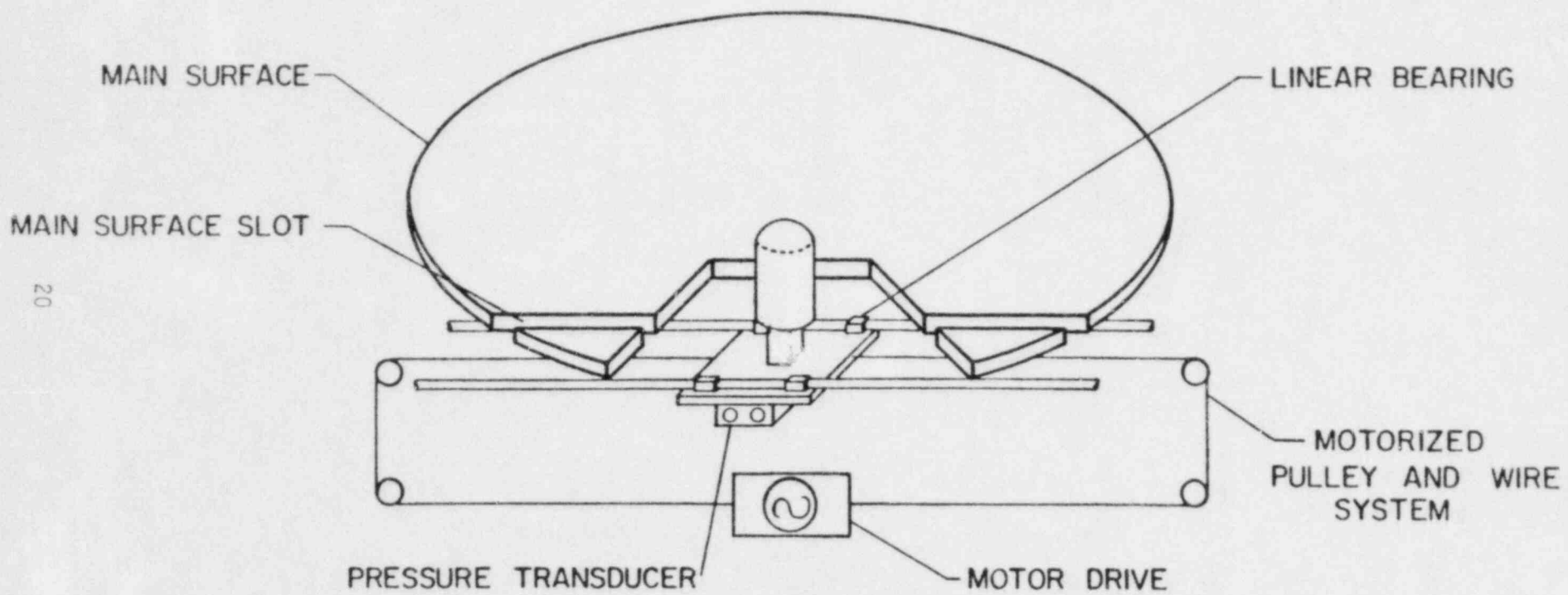PRESSURE TRANSDUCER

MOTOR DRIVE

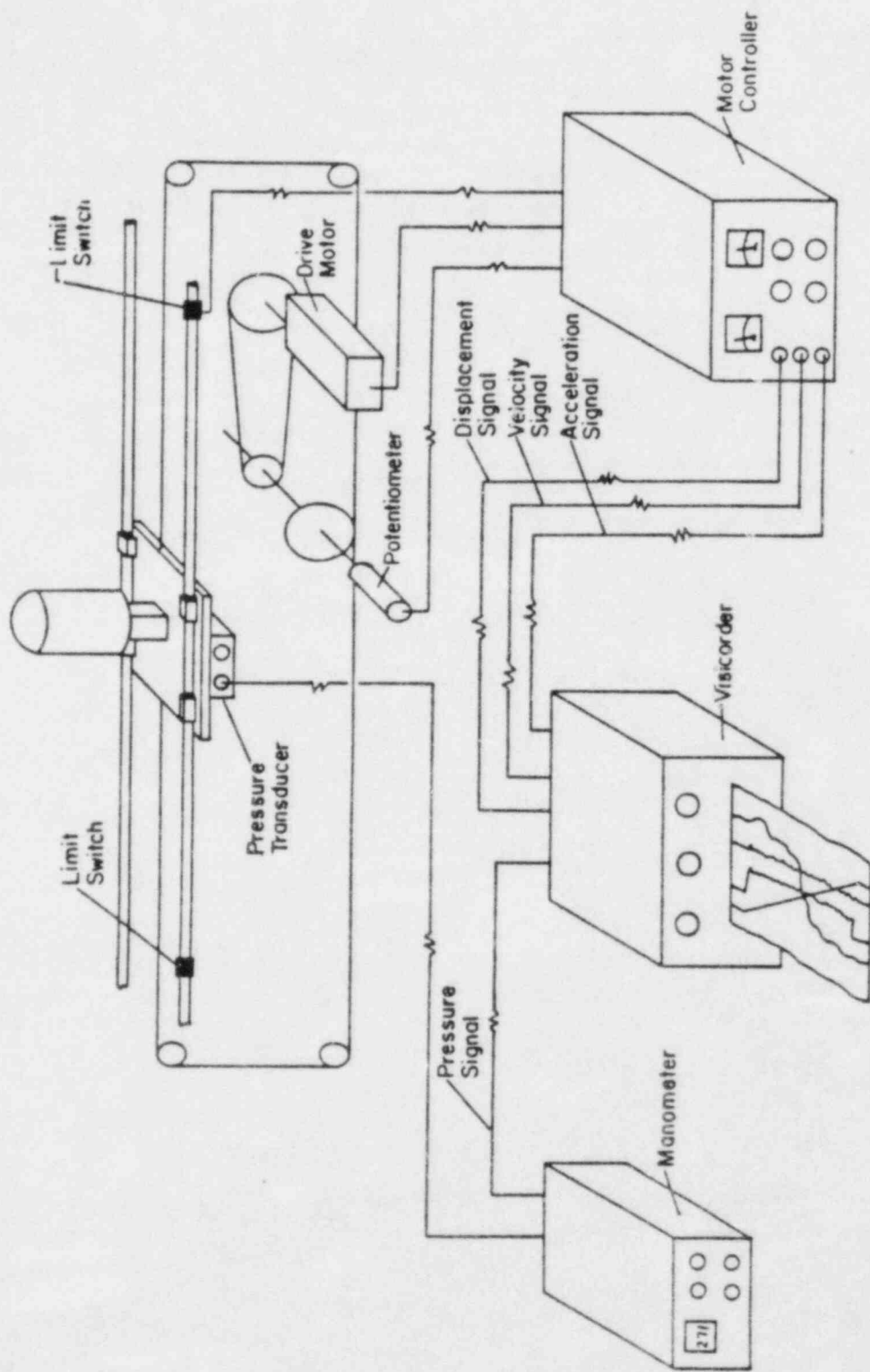Figure 4. The translation mechanism (Light, 27).

Figure 5a. Schematic diagram of the instrumentation.

21
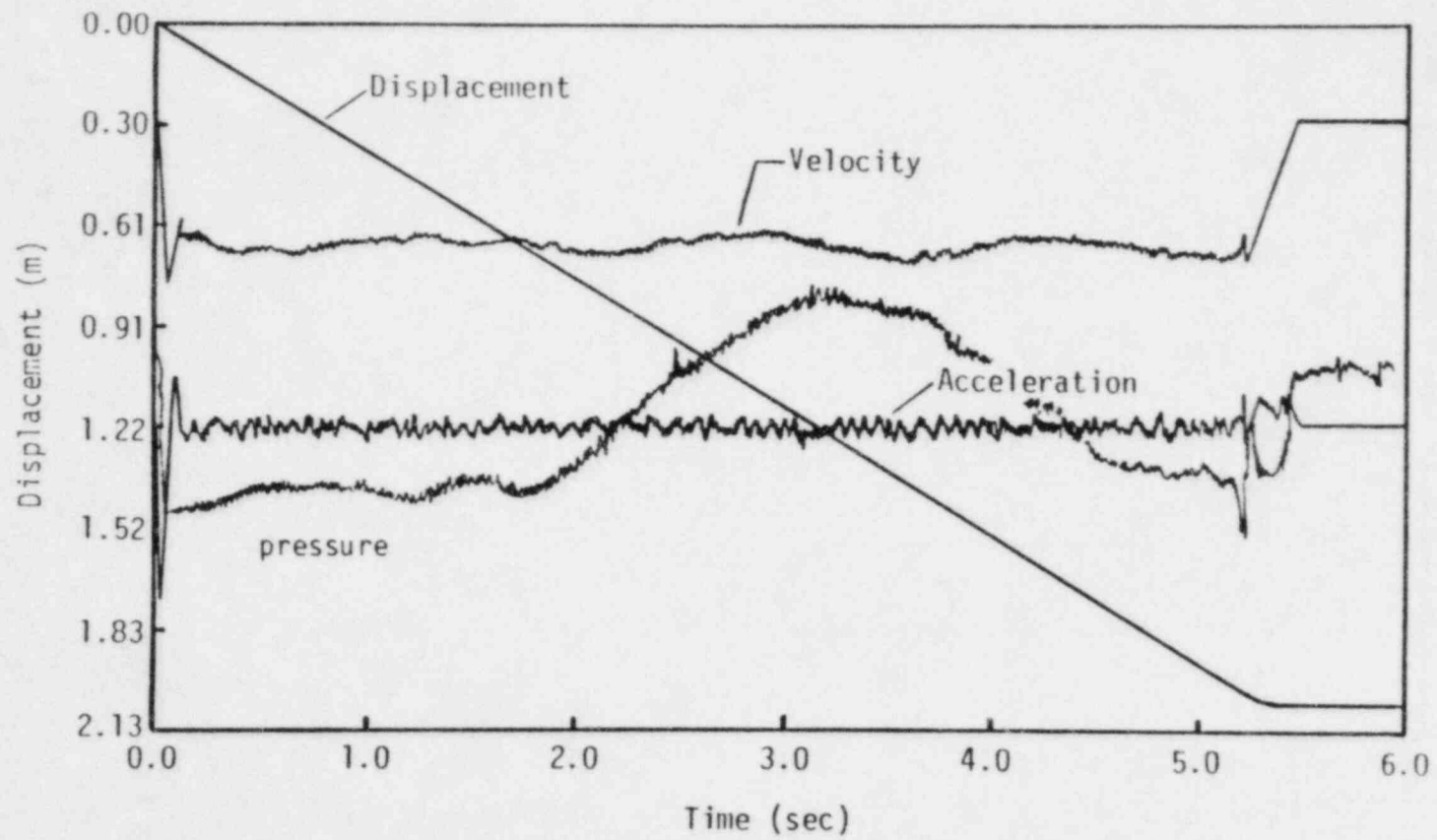
Figure 5b. Sample output from the visicorder.

22

signal from the manometer is also sent to the scope. A second series of spikes are displayed which represent the output. By comparing the time interval between the spikes, we can measure the input and output frequencies. Using this procedure, a variety of pressure-measuring set-ups were tested. As it turned out, the time response of the system is very sensitive to the length of the tubing, carrying the pressure signal, and fluid-switching mechanisms. This is one of the reasons why the transducer was carried with the model. Moreover, fluid-switches could not be used due to the slow response of the system. As a result the procedure became considerably more tedious. After each measurement, the transducer was disconnected, and reconnected to another pressure port. Figure 6 shows the time response of the system for a variety of experimental conditions.

Another quantity of interest is the velocity field. These measurements were done by hot film anemometry. The velocity profile was measured in the convergence zone. Once the volumetric flow rate is determined from the velocity data at a particular radius, conservation of mass enables one to determine the average radial velocity at any other radius. Therefore, several measurements were made at approximately the same radius to determine the volumetric flow rate, and the velocity profile (Figure 7). No attempts were made to determine the radial dependence of the velocity profile.
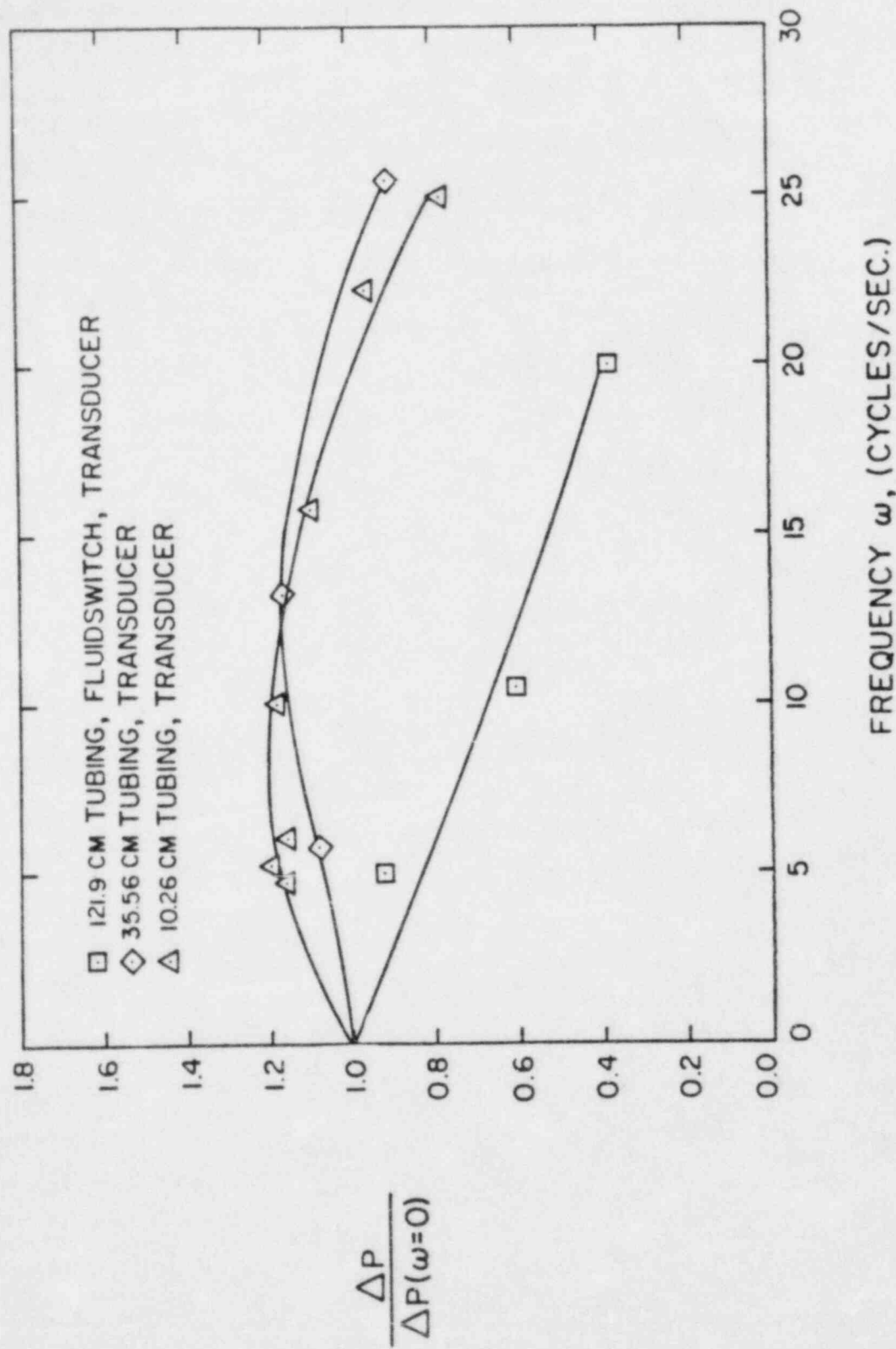
Figure 6. Frequency response under a variety of conditions.

□ 121.9 CM TUBING, FLUIDSWITCH, TRANSDUCER

◇ 35.56 CM TUBING, TRANSDUCER

△ 10.26 CM TUBING, TRANSDUCER

$$\frac{\Delta P}{\Delta P(\omega = 0)}$$

FREQUENCY ω, (CYCLES/SEC.)

24
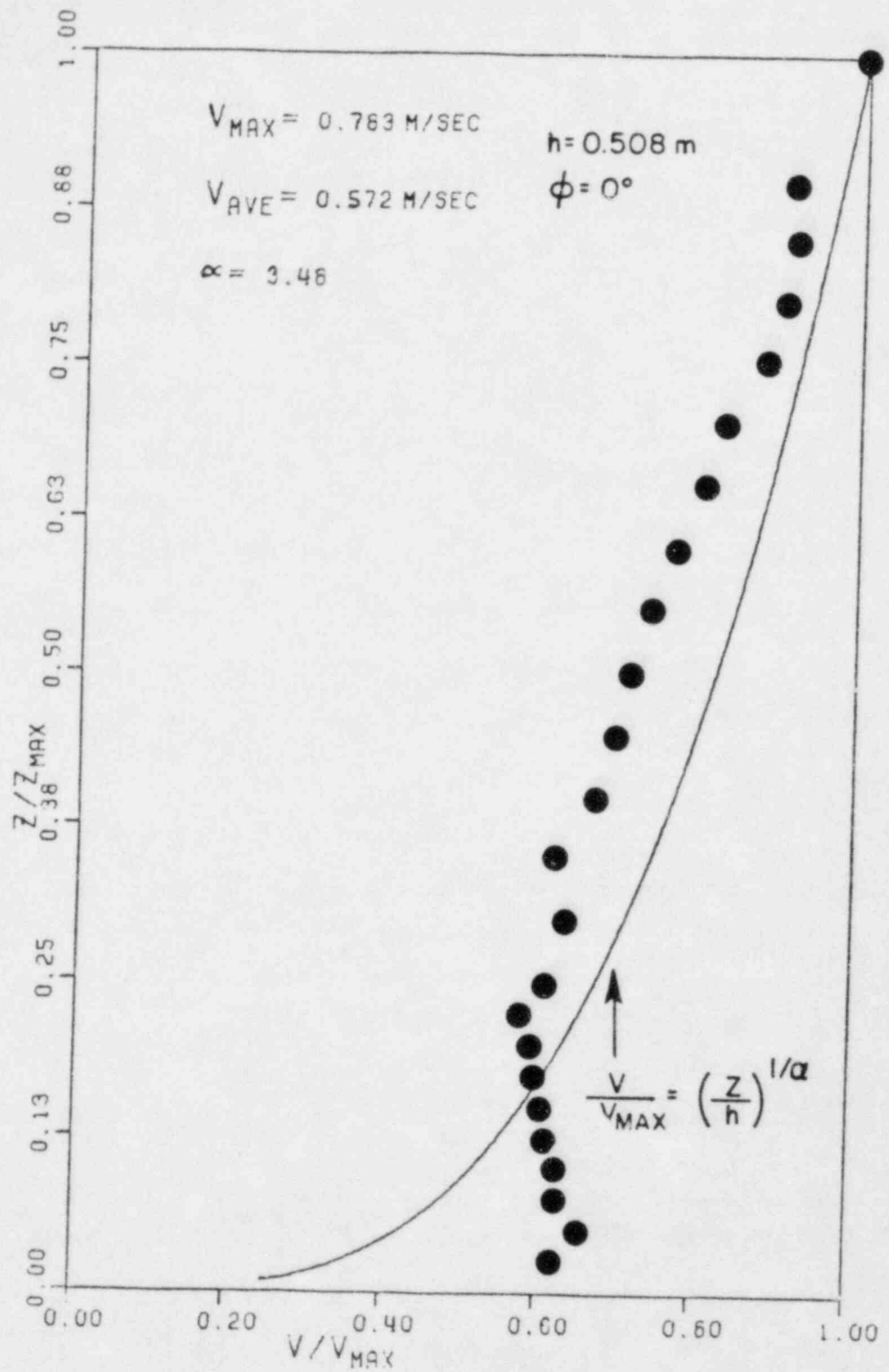
Figure 7. A typical velocity profile in the convergence zone.

25

CHAPTER III

EXPERIMENTAL RESULTS AND ANALYSIS

3.1 Pressure Coefficients

Steady and unsteady cases of tornado-structure interactions
are studied separately. As we shall see, there are significant differ-
ences between these two cases. Therefore, by comparison, we will
attempt to gain an understanding of the effects due to the translation
of the structure through the flow.

The difference between the pressure on the model and the atmo-
spheric pressure, normalized by the dynamic pressure based on the aver-
age velocity, is defined as the pressure coefficient. The normaliza-
tion factor is based on the average velocity in the region between the
screen and the core. As we shall see in subsequent sections, one of
the simplest models for the flow is the combined-Rankine vortex model,
in which the radial velocity varies as r^{-1} outside of the core region.
The average radial velocity between the screen and the core, using mean
value theorem, is

$$u_{ref} = \frac{constant}{r_s - r_c} \ln \left(\frac{r_s}{r_c} \right) \tag{7}$$

where the constant is determined experimentally.

Pressure was measured at 21 different locations on the model.
Figure 8 shows the locations where pressure was measured.

26

Z=22.13 cm

Z=20.79 cm

Z=18.66 cm

Z=16.83 cm

Z=12.86 cm

Z=8.89 cm

Z=4.92 cm

Z=0.95 cm

11.40 cm

22.86 cm

Figure 8. The model and the location of the pressure ports.

27

Thus, the experimental data consists of steady and unsteady
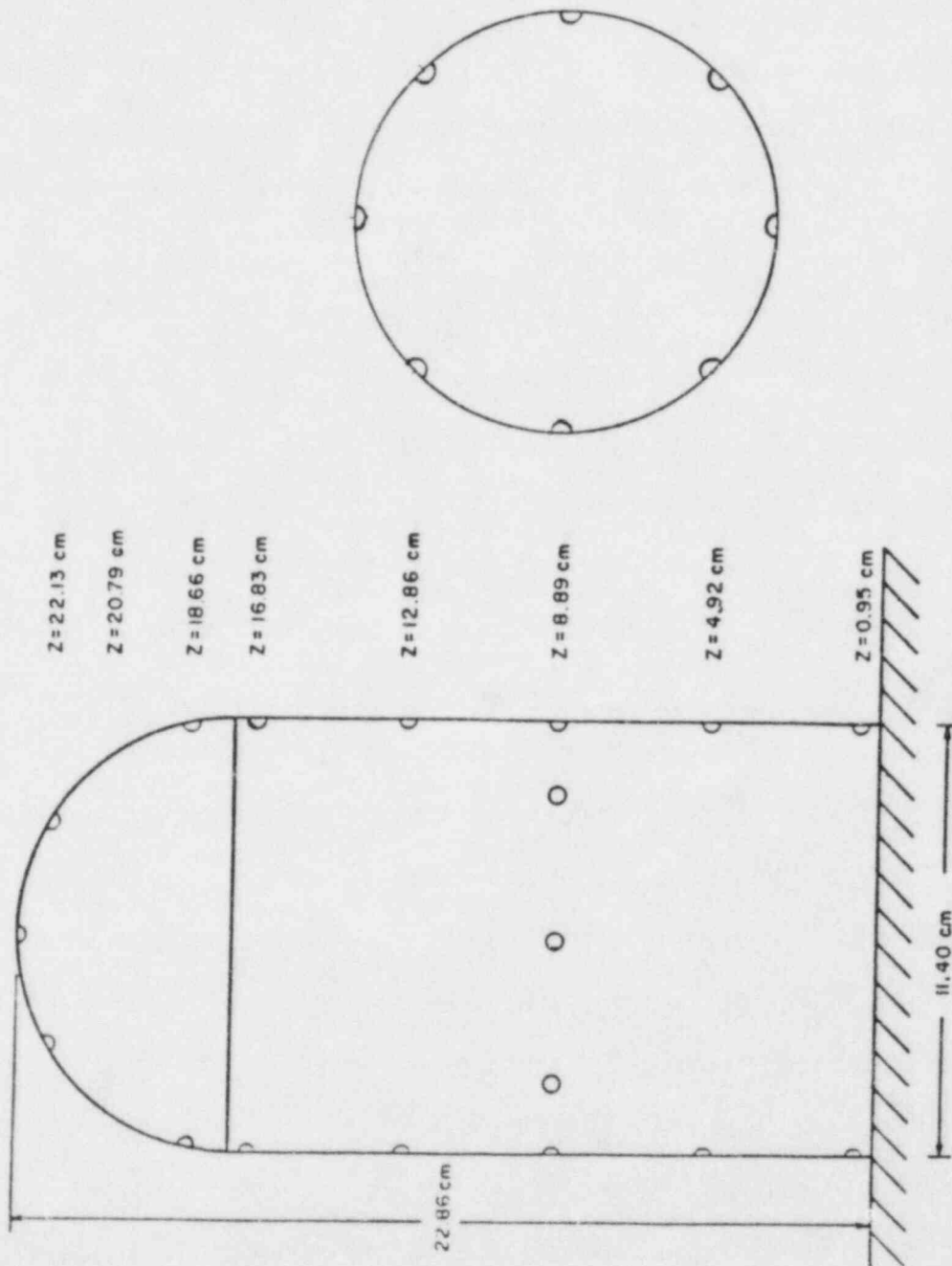sectional pressure coefficients, at 0° and 45° swirl angles. Swirl
angle is defined as the angle between the velocity vector and the
radial line. The data are recorded at 11 different locations within
the simulator, figures 9a through 9d. Before this set of data is
discussed, let us consider the flow conditions. The background flow is
not constant in the radial direction. As the flow approaches the
center of apparatus it accelerates. Therefore, the Reynolds number
based on the local flow velocity increases as we get closer to the
center. Furthermore, as the cylinder enters the convection zone, the
axial component of velocity becomes significant, and the flow is fully
three-dimensional. For the steady case, the Reynolds number based on
the local velocity of the flow and the radius of the cylinder increases
from about 3×10^4 at the screen to about 4×10^5 at the core radius,
assuming a combined-Rankine model for the flow. But, in the convection
zone, the flow does not accelerate according to r^{-1}, due to the axial
component of velocity. Another point to keep in mind is the large
amount of shear introduced at the screen, which results in significant
variations of velocity, and consequently pressure, in the axial
direction.

In the previous chapter, it was argued that the weak dependence of
the flow on the Reynolds number, and the addition of shear and rough-
ness made it possible to produce a laboratory simulation of the
"tornadic flow field". It is extremely important to bear in mind that
the same arguments cannot be used to justify a dynamically similar
"tornado-structure interaction".

28

Figure 9a. Sectional pressure coefficients on the model at different locations with respect to the position of the model relative to the vortex, steady flow, $\phi = 45°$.

Figure 9b. Sectional pressure coefficients on the model at different locations with respect to the position of the model relative to the vortex, unsteady flow, $\phi = 45°$.

Figure 9c. Sectional pressure coefficients on the model at different locations with respect to the position of the model relative to the vortex, steady flow, $\phi = 0°$.
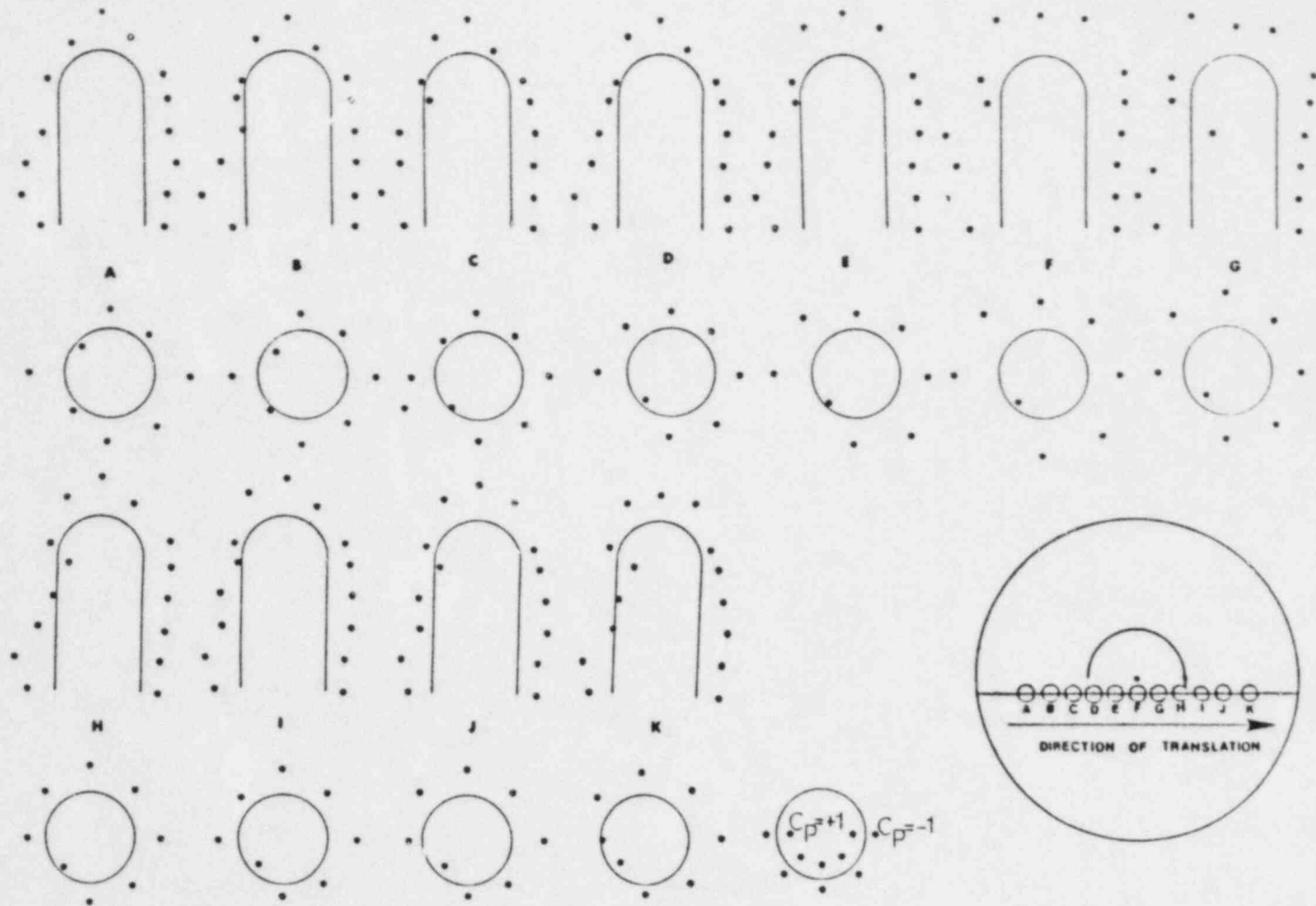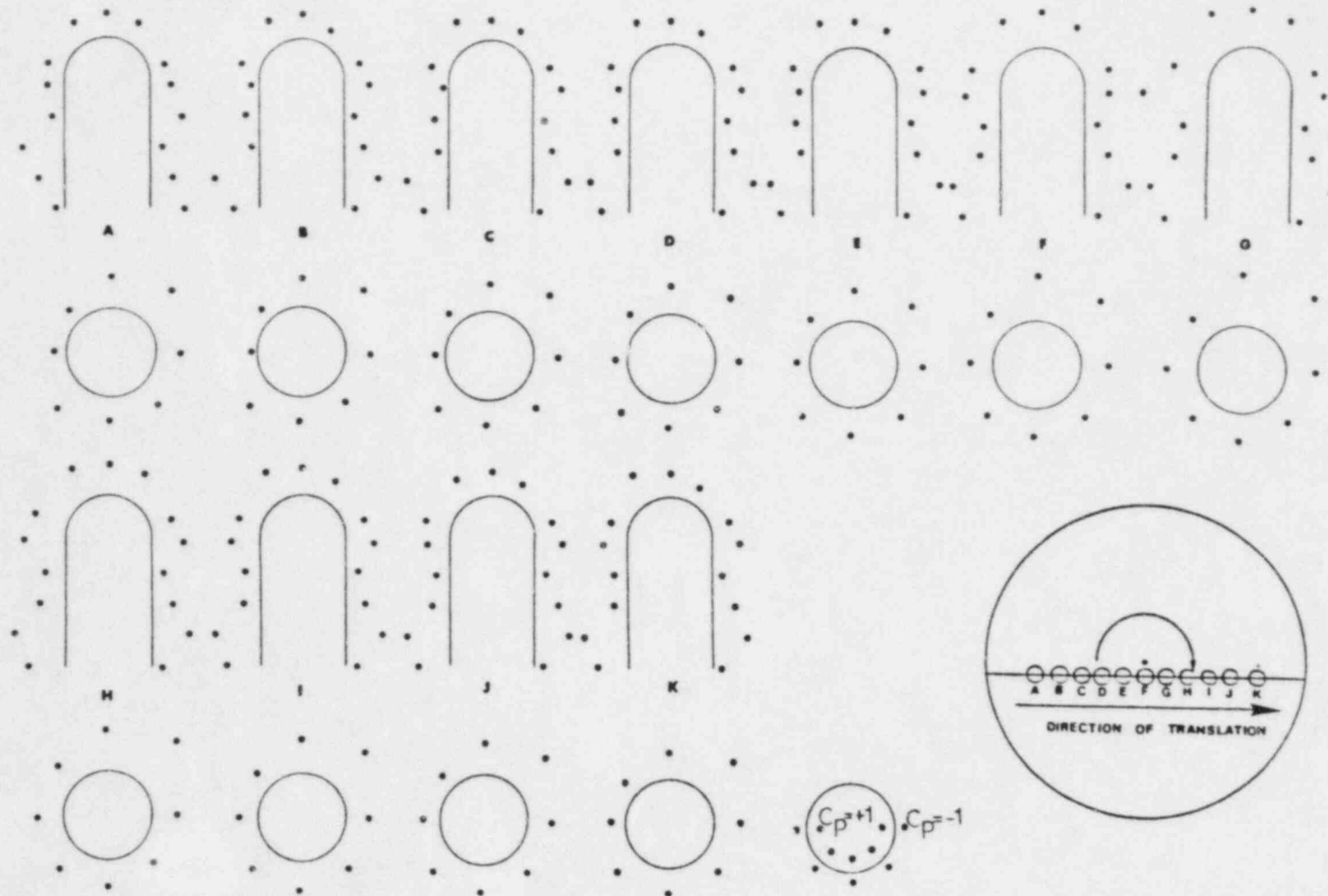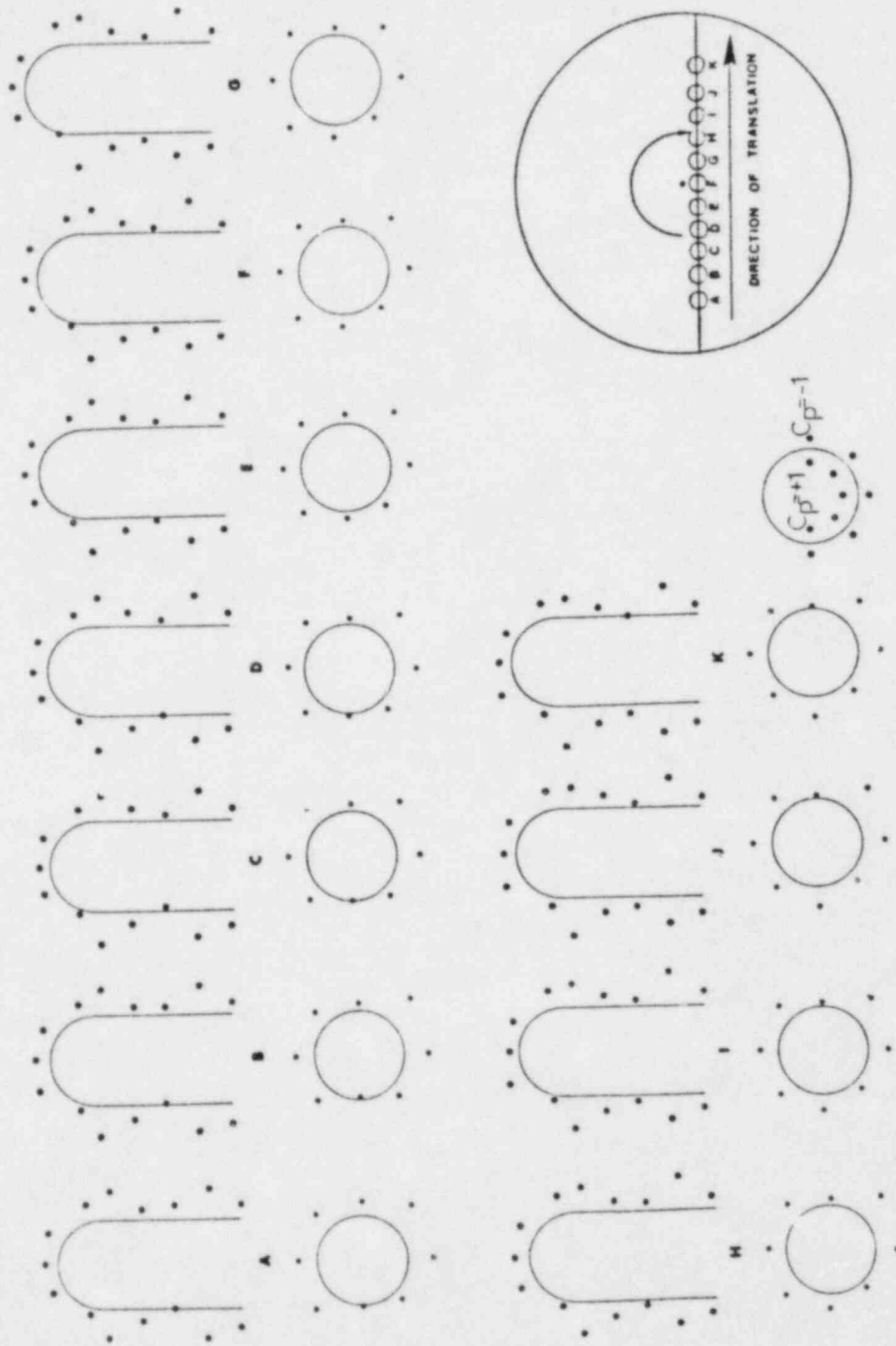
Figure 9d. Sectional pressure coefficients on the model at different locations with respect to the position of the model relative to the vortex, unsteady flow, $\phi = 0°$.

We will first study the general features of our results. The pressure coefficients show significant variations along the vertical direction on the model. This feature is primarily due to the existence of strong shear in the velocity profile. As the flow approaches the model, it slows down, and therefore, the static pressure increases. The flow, essentially, becomes a boundary layer flow in an adverse pressure gradient. This in turn, results in flow separation. The separated flow moves downward on the surface of the model, and toward the ground. This secondary flow is again a boundary layer flow with an adverse pressure gradient for the same reasons, and a separation in the secondary flow follows. Figure 10 shows the formation of "vortex cells" due to this mechanism. The vortices formed ahead of the cylinder bend around it to produce "horseshoe vortices". This is an important realization. As we shall see in the next chapter, the azimuthal vorticity of the background flow is decoupled from the other two components of vorticity. However, the addition of the cylinder to the flow, and the formation of a horseshoe vortex provides a mechanism for converting azimuthal vorticity into radial vorticity.

As the flow moves over the dome, it accelerates, which causes a low pressure region on the dome section. When the cylinder is placed in the convection zone, the existence of an axial component of velocity causes a further drop in pressure on the dome. The three dimensionality of the flow, and the cylinder-hemisphere combination, which make up the model, result in a very complex wake behind the cylinder.

In order to develop an understanding of the translational effects, let us focus our attention on the translational pressure coefficient
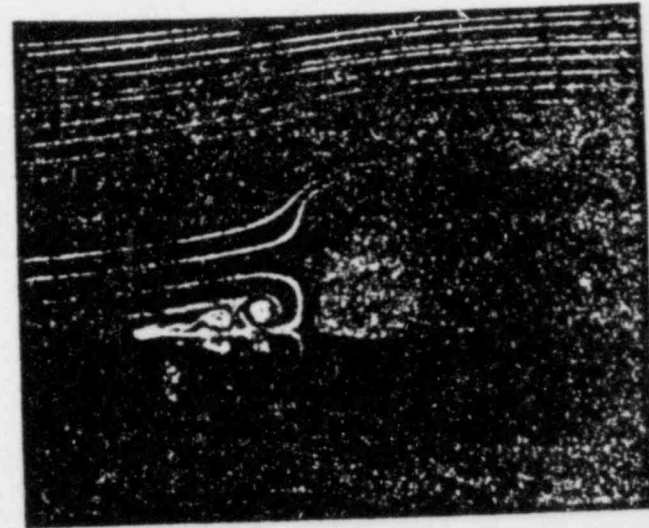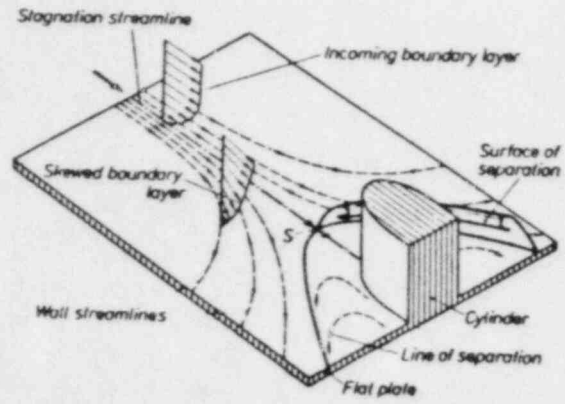
33

34

Figure 10. Vortex cell formation ahead of the cylinder (Schlichting 38).

defined as the difference between the steady and unsteady pressure co-
efficients. Figures 11a and 11b show the translational pressure co-
efficients corresponding to the swirl and purely radial flow cases, re-
spectively. As we study the translational pressure coefficients, we
note that the pressure coefficient increases in the direction of
motion. At the same time, we notice that it decreases along the
direction which makes a 45° angle with respect to the path of transla-
tion. Before we investigate this situation, let us recall that for a
cylinder translated in a stationary flow, the pressure coeffic ent
should rise in the·direction of the translation and it should decrease
along the direction perpendicular to the path of translation.

A discussion of the flow past a rotating cylinder is given by
Goldstein (37). In such a flow, the stagnation points approach one
another, causing the pressure distribution on the cylinder to change.
A comparison between the steady and unsteady pressure coefficients
around the cylinder shows significantly different pressure distributions,
figures 9a through 9d. The unsteady results are associated with a
larger pressure drop, while exhibiting a more symmetric distribution
around the cylinder. It is important to note that according to our
definition of the pressure coefficient, for a reference velocity of 50
m/s, a pressure coefficient of order of unity corresponds to a pressure
drop of about 0.2 psi, and for a reference velocity of around 100 m/s,
the pressure drop is about 1 psi. Taking into account the very large
area over which this pressure difference acts, the net force acting on
the structure is very large. More discussions on the forces acting on
the structure will follow in the next section. The important feature is
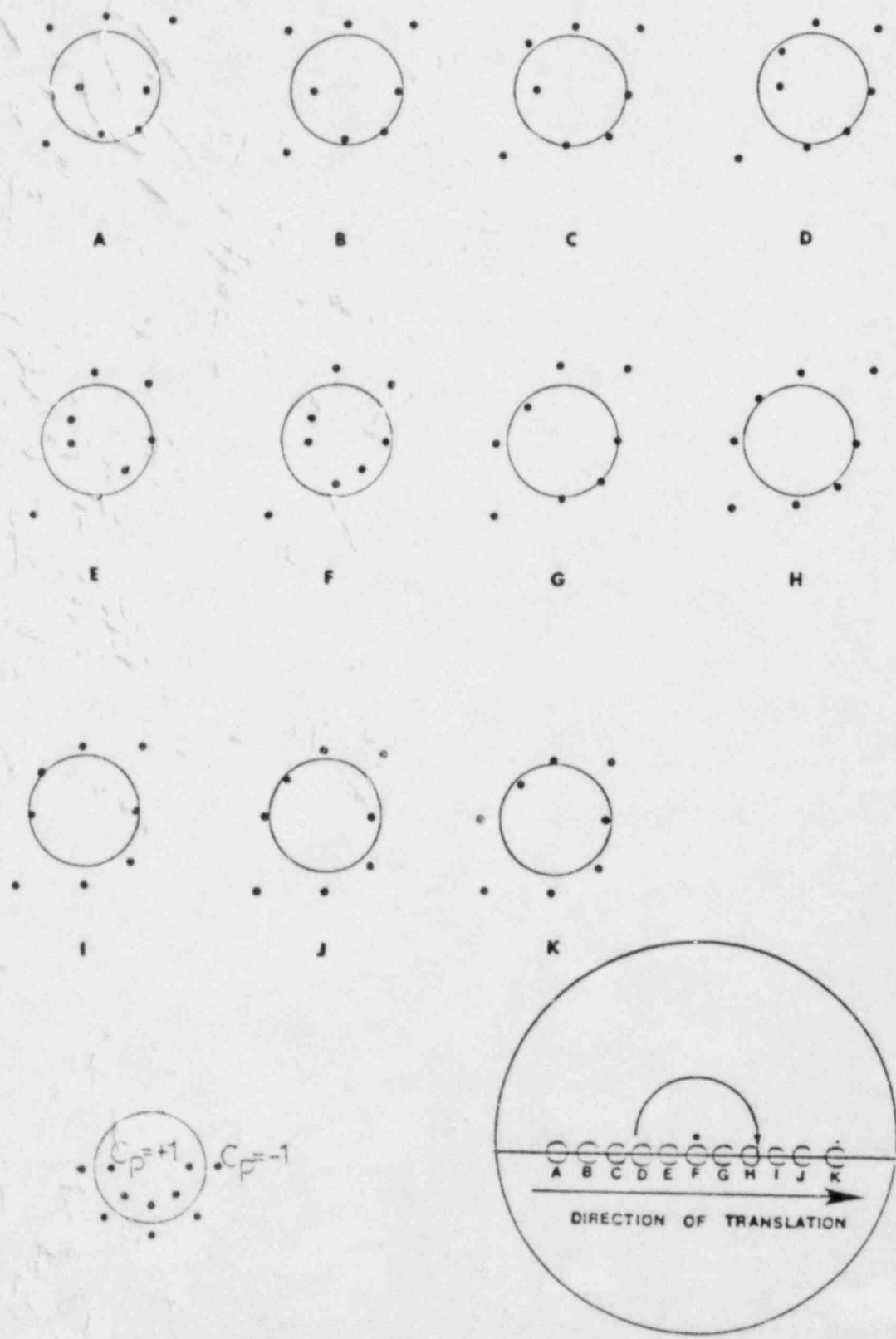
35

Figure 11a. Translation pressure coefficients, φ = 45°.
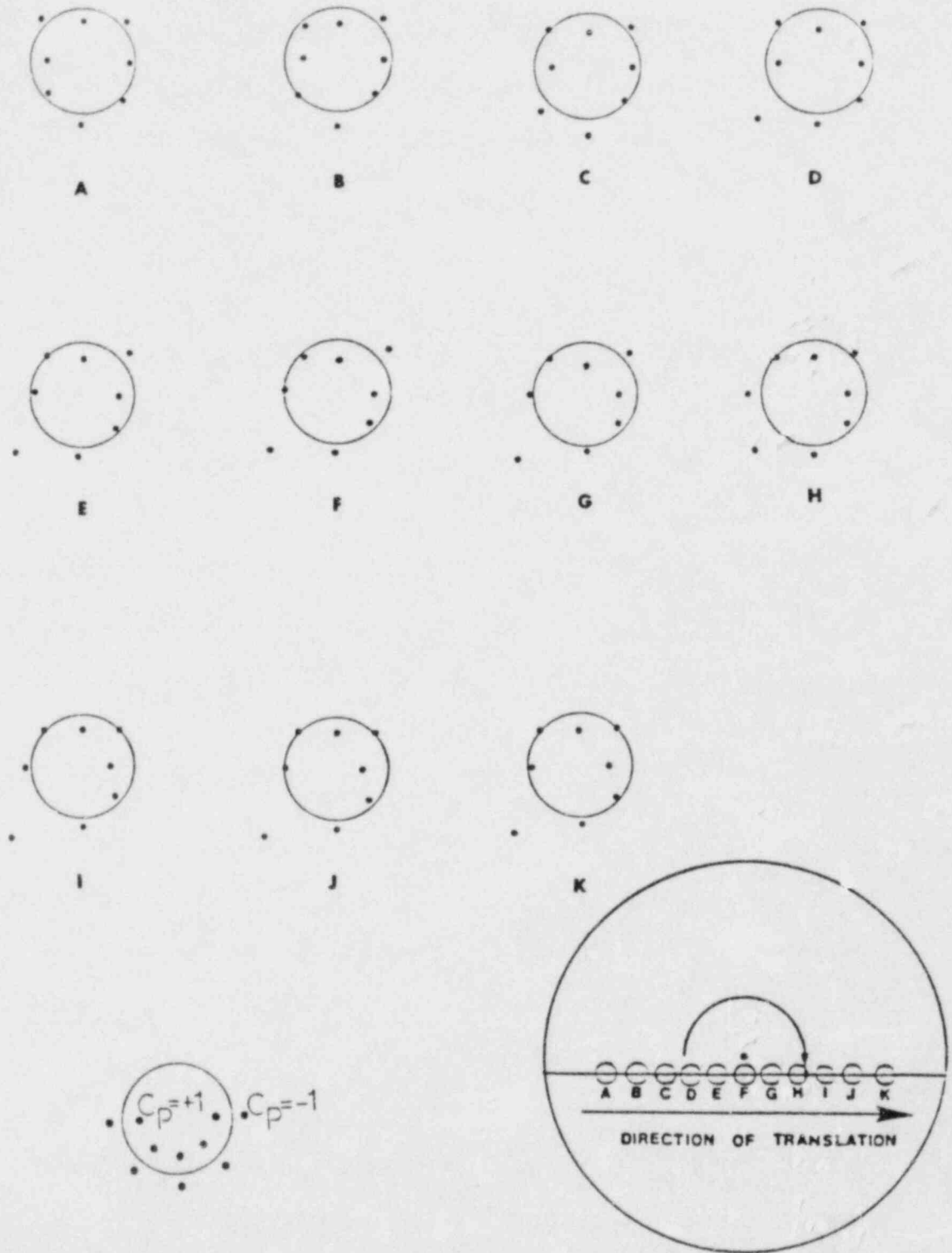
Figure 11b. Translation pressure coefficient, $\phi = 0°$.

37

the side force (lift) due to the presence of a circulation around the cylinder. This additional side force contributes to an increase in magnitude, and alters the direction of the steady force, by redistributing the pressure.

A different interpretation of the translational sectional pressure coefficients is possible by considering the motion of a cylinder in a fluid undergoing rigid body rotation. Since the flow outside the core region is not in rigid body rotation, such an idea may seem irrelevant, at first. However, if we consider the distribution of circulation to be the dominant factor, then it is possible to consider an equivalent rigidly rotating flow, having the same local circulation. As described by Greenspan (23), the motion of a cylinder along a path perpendicular to the axis of rotation produces a cross flow over and around the cylinder. The translational sectional pressure coefficients represent a distribution similar to the case of a cylinder in a cross flow. Once again we arrive at the same conclusion which is an additional side force due to translation.

Earlier, we discussed the formation of horseshoe vortices ahead of the cylinder. During translation, these vortices get stretched and intensify. This effect is evident in the plots of the pressure coefficient in the axial direction (Figures 9a through 9d). The variation of pressure in the axial direction for the unsteady case is far more pronounced than for the steady case. As we mentioned earlier, one of the unsteady effects seems to be a stronger drop in pressure on the surface of the model. This phenomenon may contribute to the mode of failure

known as "bursting", in which the difference between the internal and external pressures may cause the structure to burst.

The only other experimental data regarding this experiment is due to Jischke & Light (10), who studied the steady effects. Figure 12 shows a comparison between the results of these two experiments. Pressure coefficients for the steady flow at a swirl angle of 45°, with the model at a distance of 0.76 m have been chosen for this comparison. It should be pointed out that the differences between the pressure coefficients have been exaggerated. A common value has been subtracted from both plots to enhance the subtle differences. The main difference between the two graphs is the behavior of pressure at 90° with respect to the local direction of the flow. For a cylinder in a potential flow, pressure falls to a minimum value at this location. Our experimental results show a slight rise in the pressure coefficient at 90° to the local direction of the flow. Since the data were obtained at only eight locations around the cylinder, one cannot compare the two cases in a meaningful fashion. In addition, Jischke & Light reported the uncertainty of their resu 's at 29%, and the standard deviation of our results from their results is about 25%. Therefore, statistically, there are no significant differences between the two.

3.2 Force Coefficients

In the absence of strong body and viscous forces (high Reynolds number), the force acting on the cylinder is primarily due to pressure. Integration of pressure on the surface of the body determines the forces acting on the body. We adopt a coordinate system fixed to the
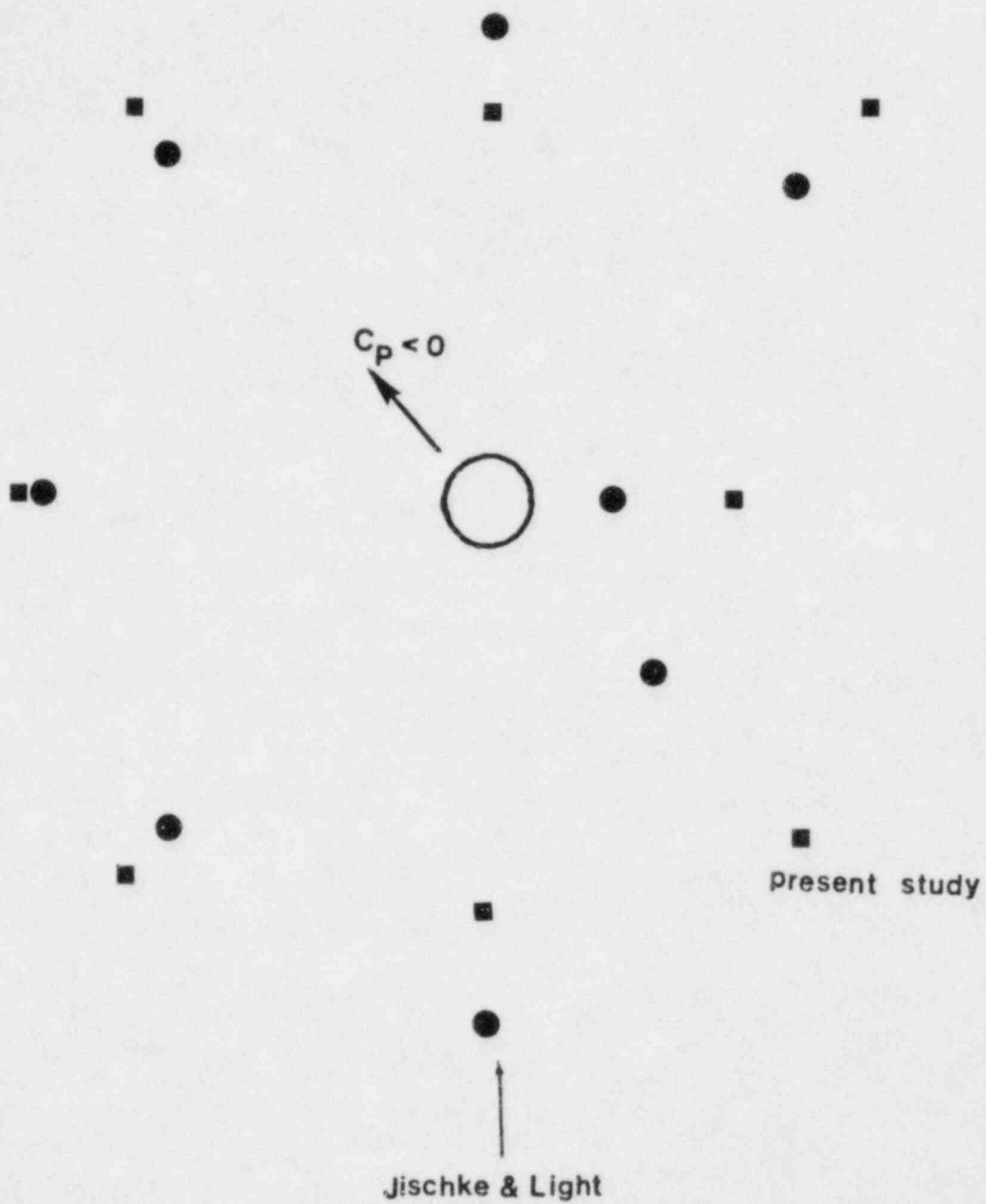
39

Figure 12. A comparison between the results of the present study, and experimental results of Jischke & Light (10).

model. The X-axis is chosen in the direction of motion of the cylinder. The Z-axis is perpendicular to the floor of the simulator and pointing up, and the Y-axis is chosen such that XYZ is a right-handed coordinate system.

To avoid some of the enormous complexity of this fully three dimensional, unsteady, turbulent shear flow around a cylinder with a hemispherical roof, we will initially concentrate on the calculations based on the azimuthal pressure distribution around the middle section cf the cylinder. Eight pressure coefficients are known at different locations around the cylinder. Each is multiplied by 1/8 of the perimeter and assigned a direction which is the same as the unit normal for the particular area. Then, the eight vectors are summed vectorially to obtain the net sectional force coefficient.

Figures 13a and 13b show the sectional force coefficients for the steady and unsteady cases at two different swirl ratios. Figure 15a shows a comparison between the steady and unsteady sectional force co-efficients for a purely radial flow. For the steady case the sectional force coefficient increases as the model is placed closer to the center. However, the unsteady sectional force coefficient decreases, slightly, as the model moves towards the center of the apparatus. If we consider the ratio of the magnitude of the unsteady sectional force coefficient to the magnitude of the steady force coefficient, we note that this ratio decreases as we approach the center. As the model recedes from the center the unsteady sectional force coefficient de-creases slightly. On the other hand, the steady sectional force co-efficients corresponding to the same locations continue to increase, and then decrease. As a result the ratio of the magnitude of unsteady

41

Figure 13a. Horizontal sectional force coefficient based on the azimuthal distribution of pressure around the middle section of the cylinder, $\phi = 0°$.

42
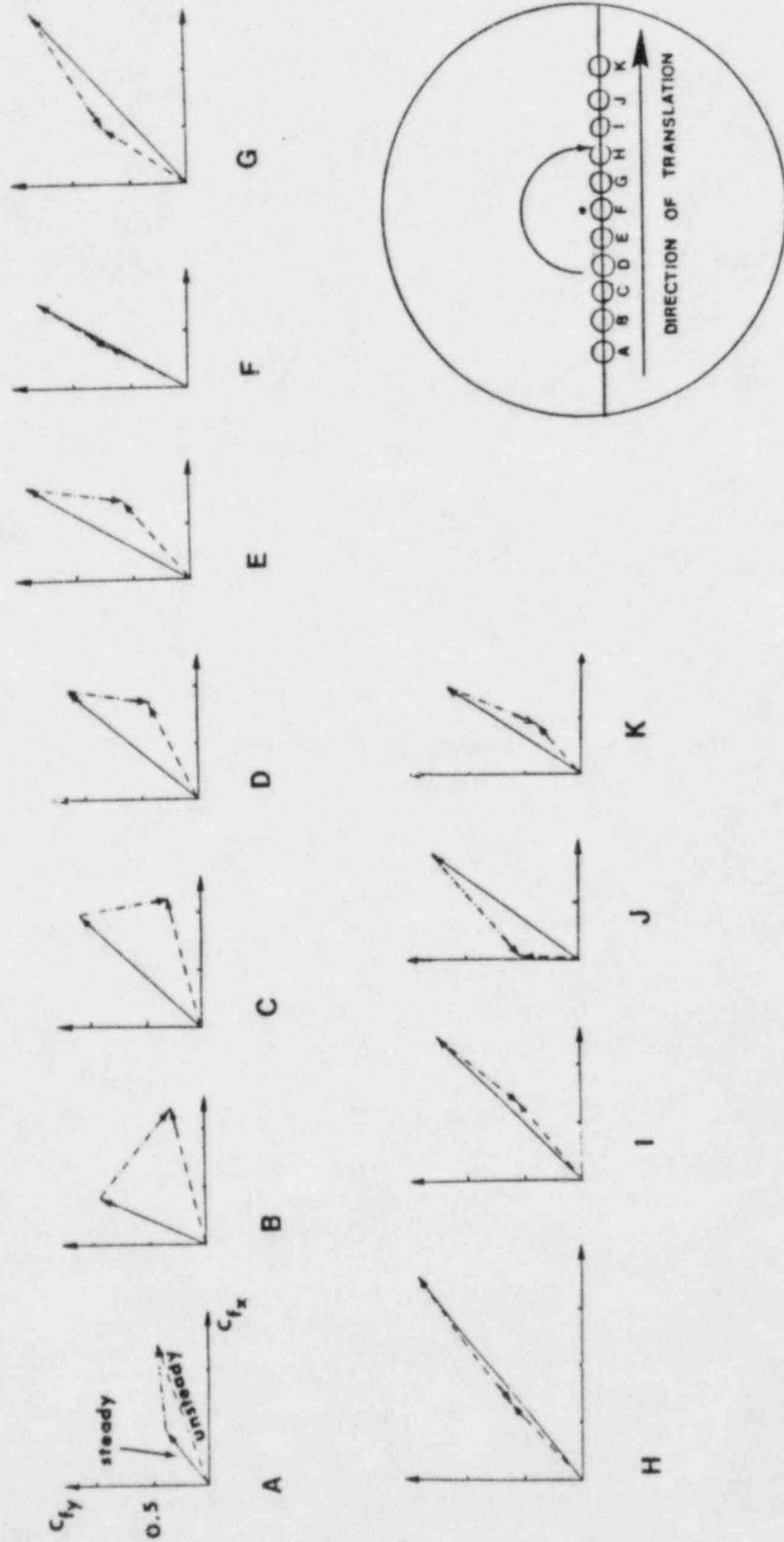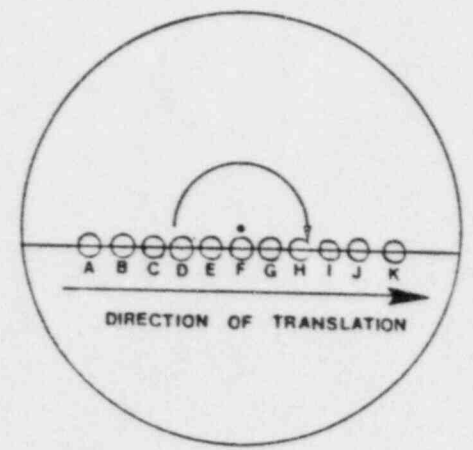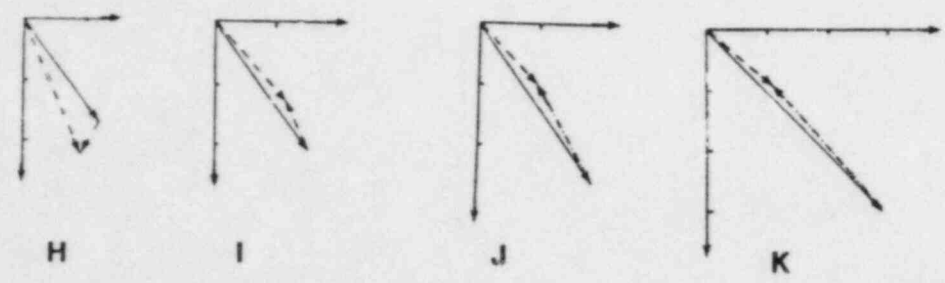
Figure 13b. Horizontal sectional force coefficient based on the azimuthal distribution of pressure around the middle section of the cylinder, $\phi = 45°$.

to steady sectional force coefficients decreases and then increases, slightly. Figure 14 shows the ratio of the unsteady to steady sectional force coefficients for radial flow, based on the azimuthal pressure coefficients around the middle section of the cylinder. Figure 16 seems to suggest that translation reduces the net force acting on the structure around the middle section of the cylinder. We already anticipated this phenomenon when it was learned that translation causes a much more symmetric distribution of the pressure on the structure.

Figure 13b shows that the steady sectional force coefficient decreases as the model is placed closer to the center. The unsteady sectional force coefficient remains relatively constant in magnitude as the model moves toward the center. As the model begins to recede from the center, the unsteady sectional force coefficient increases dramatically. Further away from the center, the unsteady sectional force coefficient decreases with increasing distance. Figure 14 shows the ratio of the unsteady sectional force coefficient to the steady sectional force coefficient for swirl flow. This ratio assumes its largest value around the center. Far away from the center the unsteady sectional force coefficient seems to be smaller than the steady sectional force coefficient. Therefore, the combined effects of swirl and translation appear to be an increase in the sectional force coefficient, especially in the vicinity of the vortex.

In figures 13a and 13b, we define the vectorial difference between the steady and unsteady sectional force coefficients as the translational sectional force coefficient. Since the x-direction is the direction of translation, we would have expected a constant trans-

44
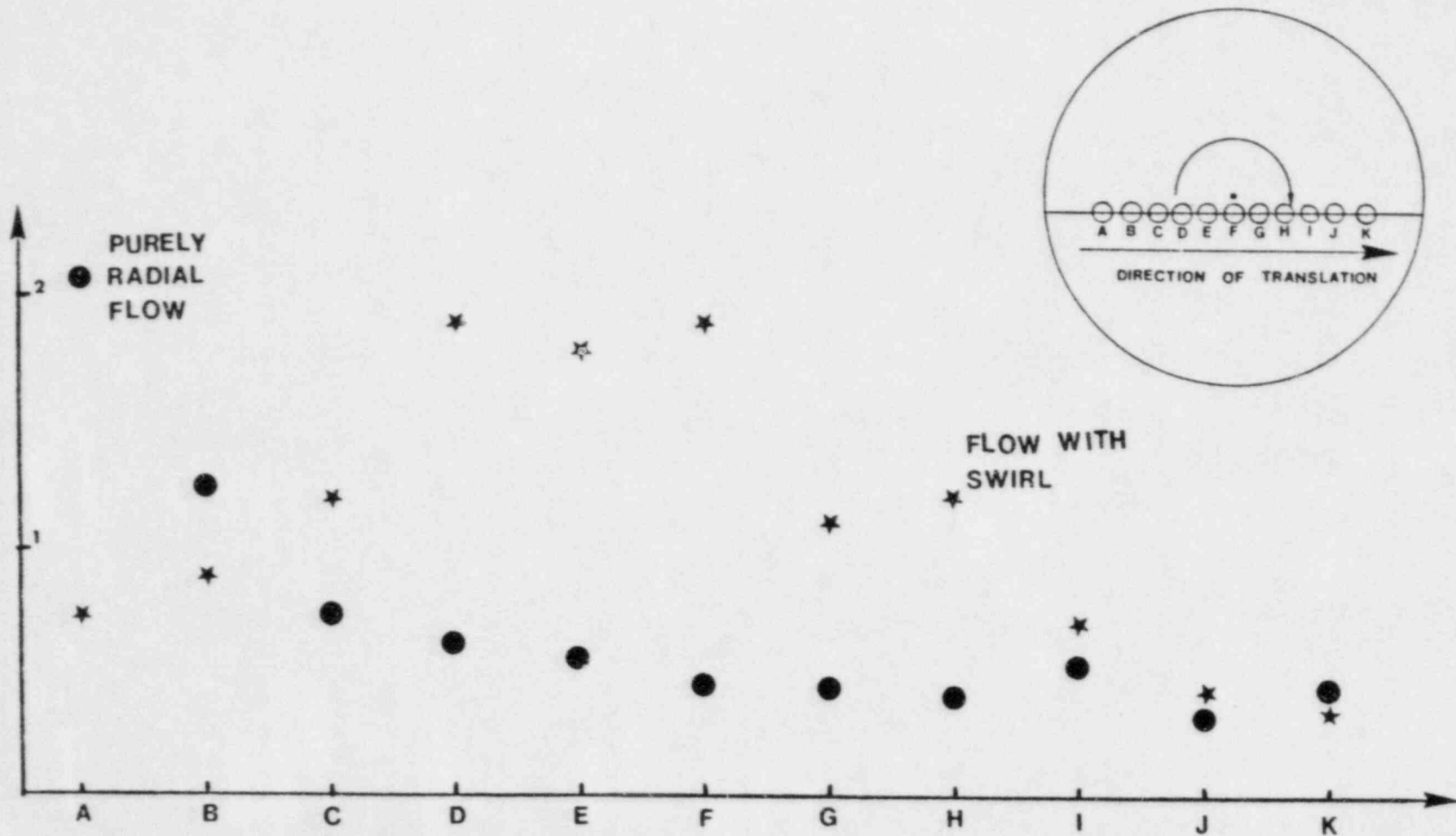
Figure 14. The ratio of the unsteady to the steady sectional force coefficient, as a function of the location of the model relative to the vortex, at swirl angles of 0° and 45°.

lational force coefficient, had it been possible to account for the translational effects by an additional drag force. But, as it is evident in figures 13a and 13b, the unsteady sectional force coefficient is neither constant in magnitude nor in direction. Thus, the foundation is laid to argue that the translational effects are significant, and we cannot take a linear combination of the steady results and the translational contribution, as calculated by placing the structure in a uniform flow, to obtain the unsteady results.

Figures 13a and 13b show the axial sectional force coefficients. These sectional force coefficients are obtained by integrating the pressure over the dome section of the model. Figure 15a contains the results for a purely radial flow. The steady sectional force coefficient gets smaller as the model is placed in the updraft region, and close to the center. The explanation of this phenomenon is the separation of the flow in the updraft region. The radial flow is an unstable flow, and particularly, in the updraft region, where the axial component of velocity gets large, flow separation follows. The existence of the region of separated flow was confirmed, by visualizing the flow field using smoke (Plate 1). The unsteady results, for the radial flow, show that initially there is a strong unsteady force coefficient, which is probably due to the impulsive motion of the model. However, as the model begins to move through the flow, the unsteady force coefficient gets very small. During this phase of the translation, the local velocity of the flow is almost equal to the velocity of the translation, and in the same direction. Therefore, effectively, the body moves with the fluid, and the relative velocity between the two is

46

47
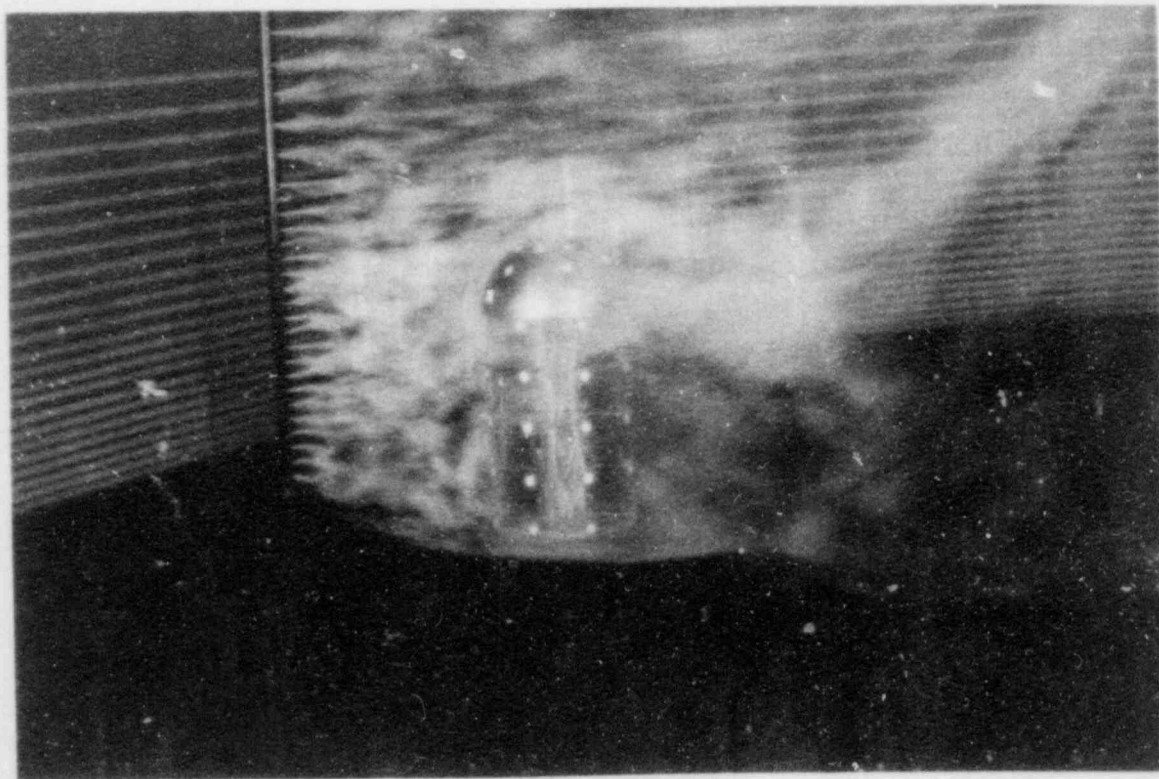
Plate 1. Photograph of the model in the visualized flow, $\phi = 0°$.

C_{f_z}

■ unsteady flow

steady flow

8

6

4

2

48

A B C D E F G H I J K

A B C D E F G H I J K

DIRECTION OF TRANSLATION
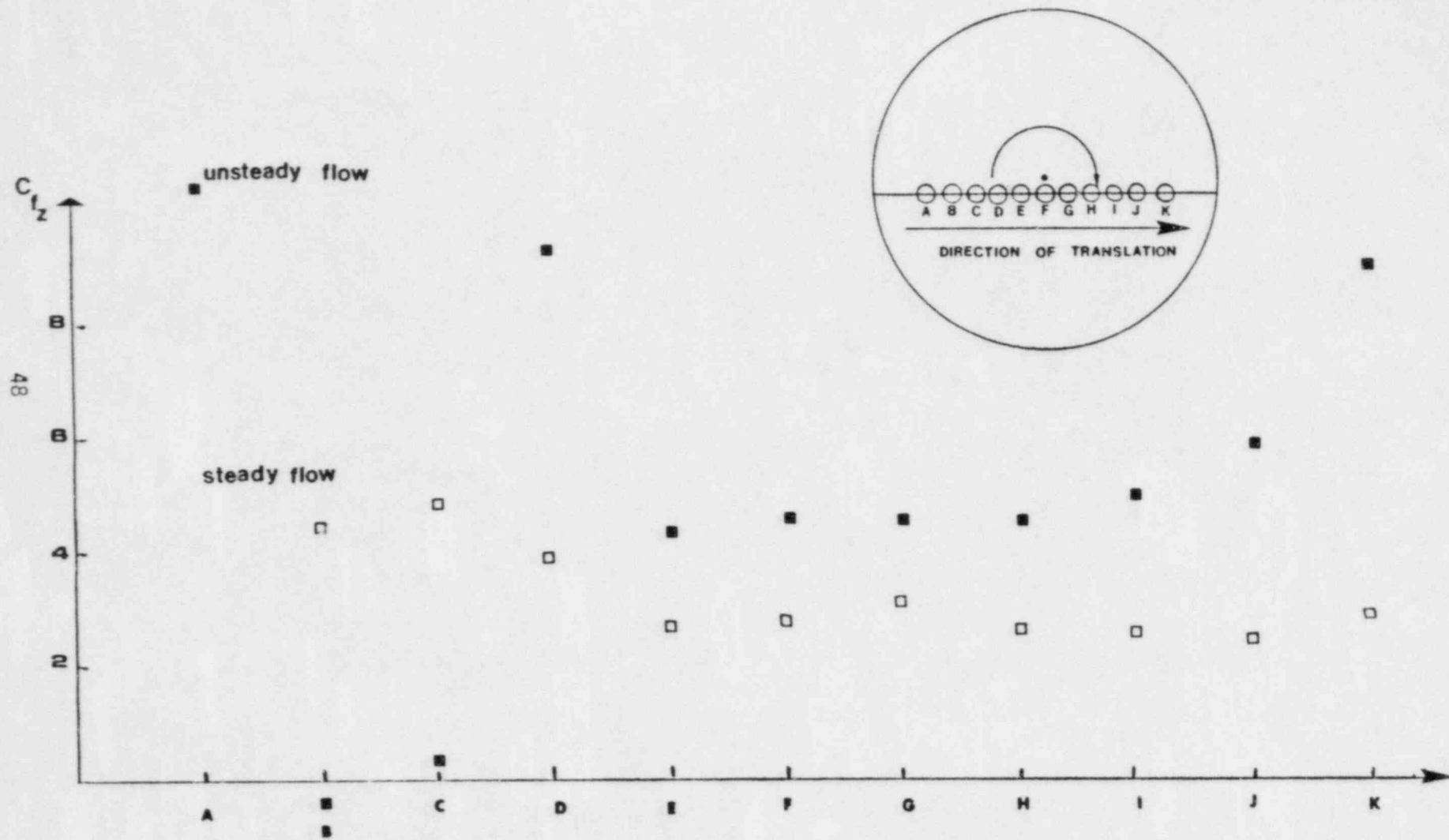
Figure 15a. Axial sectional force coefficient, $\phi = 0°$.
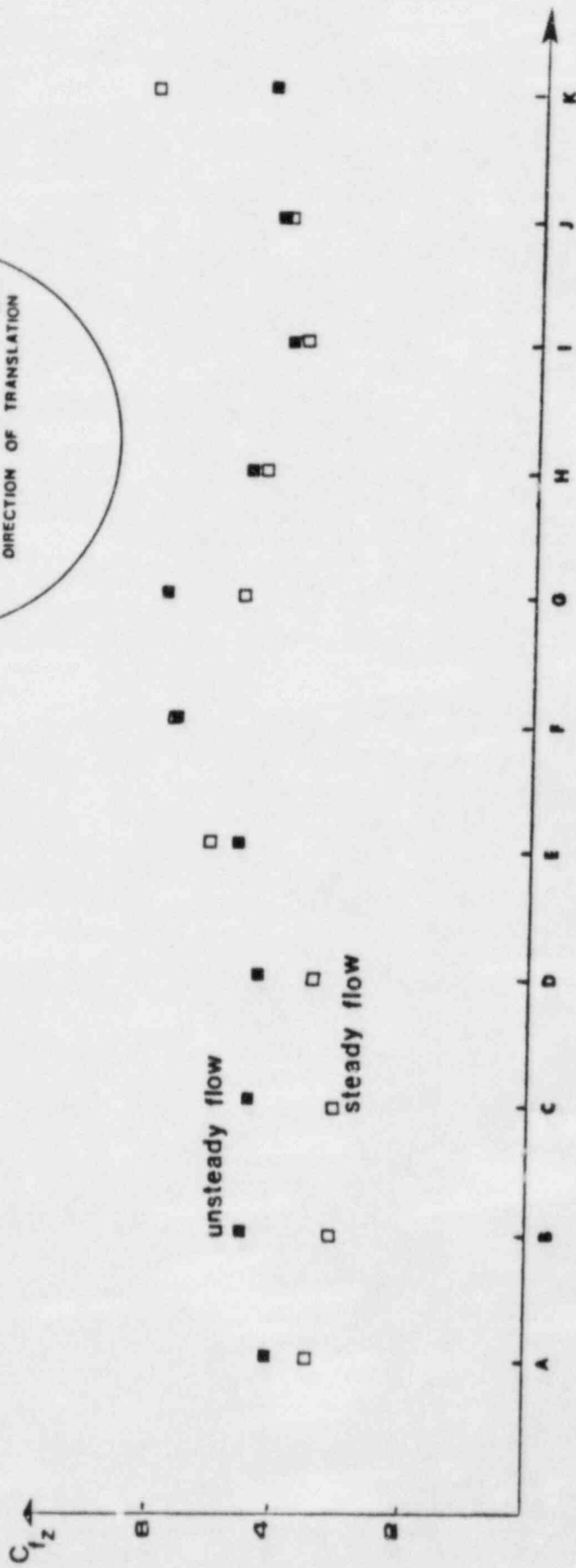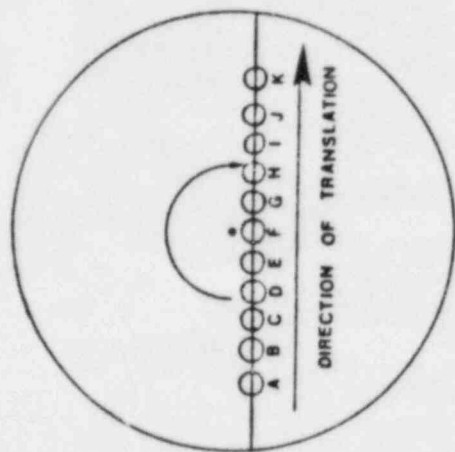
Figure 15b. Axial sectional force coefficient, φ = 45°.

very small. However, as the model enters the updraft region, the axial velocity of the flow increases dramatically, giving rise to a strong unsteady sectional force coefficient in the axial direction. As it was discussed earlier, as the model gets even closer to the center, it enters the separated flow region and the unsteady sectional force coefficient decreases accordingly. Then, the model begins to recede from the center, and leaves the separated flow region, and the unsteady force coefficient begins to rise again. As the model recedes from the center it moves in the direction which is opposite to the local flow direction. Therefore, the relative velocity between the fluid and the model is greater than the local velocity of the undisturbed flow. Accordingly, figure 15a shows that the unsteady sectional force coefficient is significantly larger than the steady sectional force coefficient, during this phase of the translation.

Figure 15b shows the sectional force coefficients for the swirl flow. In this case, the steady force coefficient obtains larger values as the model is placed closer to the center. The addition of the vortex has a stabilizing effect on the flow field. Flow visualization reveals that the swirl flow does not separate near the center (Plate 2). The steady sectional force coefficient gets considerably larger as the model is placed near the vortex. Light (27) observed, by visualizing the flow, that when an obstacle is placed in the flow, and sufficiently close to the vortex, there is a tendency for the vortex to move and attach itself to the obstacle (Plate 3).

The unsteady axial sectional force coefficient in figure 14b exhibits the same general behavior. As the model translates towards

50

51
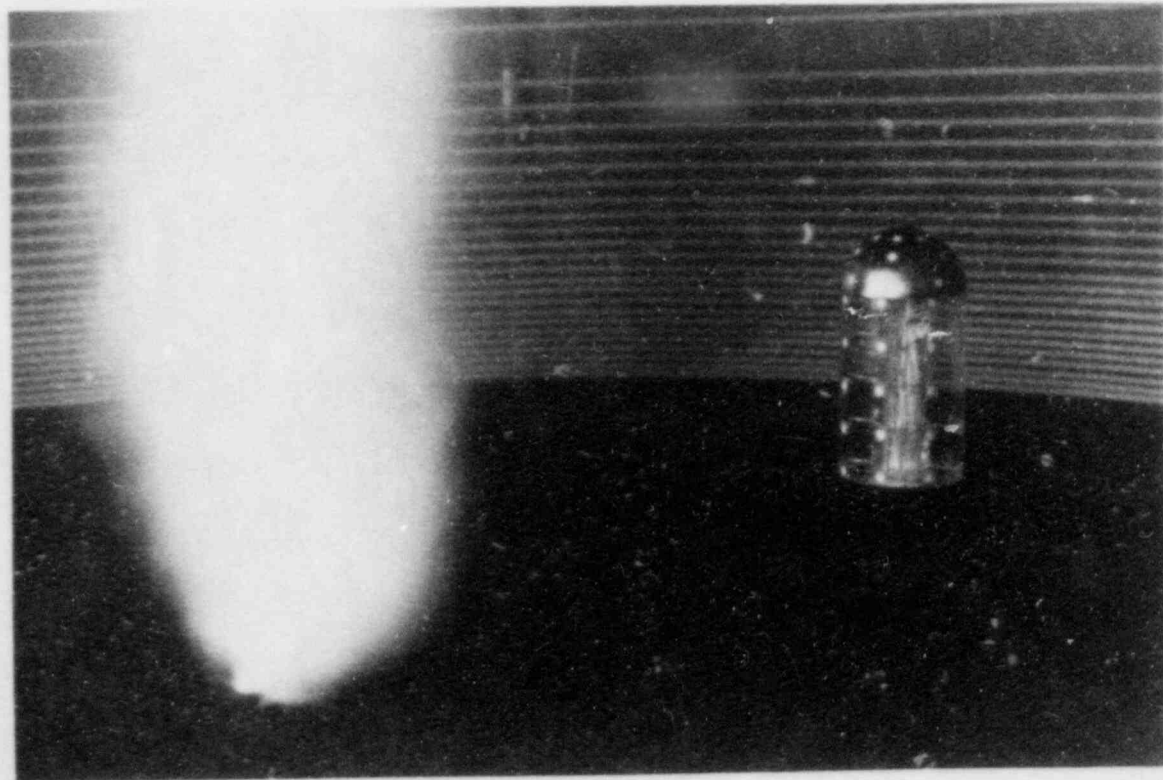
Plate 2. Photograph of the swirl flow with the visualized vortex, $\phi = 45°$.
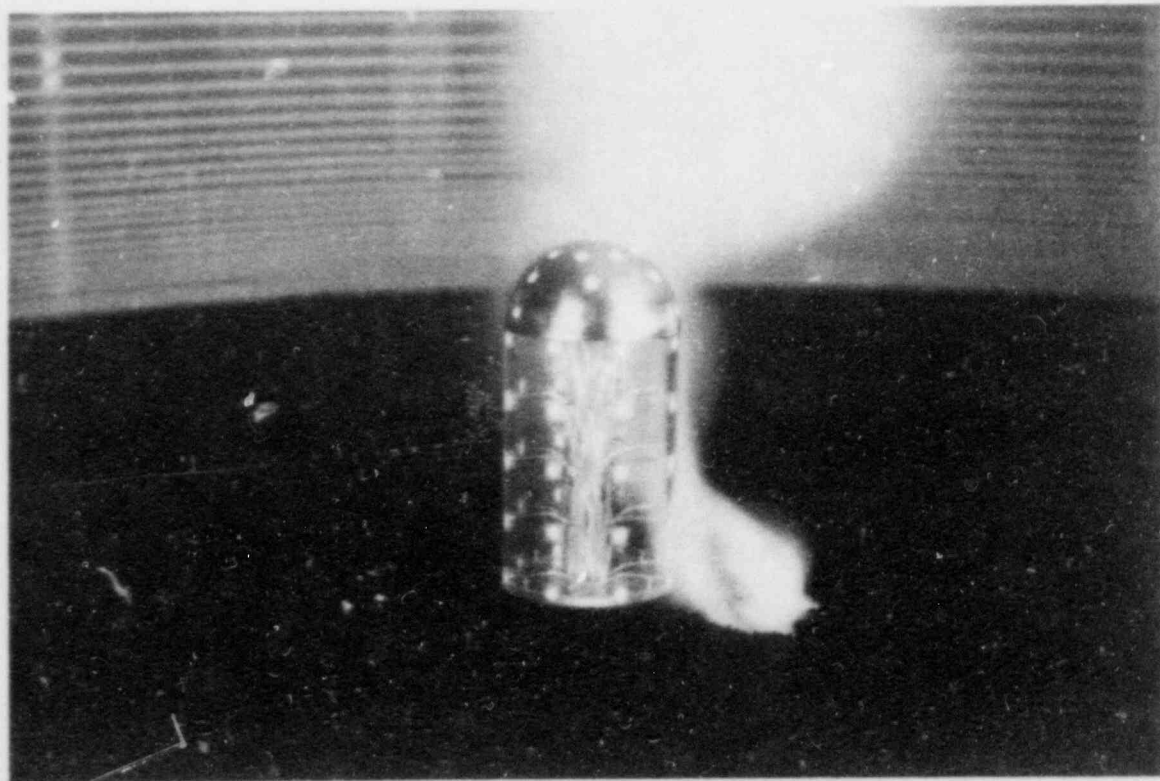
Plate 3. Photograph of the model at r = 0.11 m with vortex attachment, ϕ = 45°.

the center, the axial sectional force coefficient increases. The unsteady axial sectional force coefficient is larger than the steady axial sectional force coefficient in the covergence zone. However, as the model enters the updraft region and approaches the vortex, the steady and unsteady axial sectional force coefficients are roughly the same. Recalling from figure 15a that the unsteady results are considerably larger than the steady results, for a purely radial flow, we conclude that the contribution due to swirl has a far greater effect on the axial sectional force coefficient than the contribution due to the translation. A subtle aspect of the unsteady sectional force coefficient is that as the model passes through the vortex region, the unsteady sectional force coefficient continues to rise. In fact, the maximum value of the unsteady axial sectional force coefficient is reached shortly after the model has passed through the vortex region. Once again, we recall Light's (27) observation that once the model is sufficiently close to the vortex, the vortex attaches itself to the model. The unsteady results of figure 15b seem to indicate that the attached vortex moves with the model over a short distance, which causes the vortex to stretch. As the vortex stretches, according to Kelvin's circulation theorem, the circulation must increase, which is the reason for the larger sectional force coefficient, shortly after the model has passed through the vortex. Of course, this phenomenon does not last for long, and soon the vortex is detached from the cylinder. Figure 15b shows that after the model has receded sufficiently far from the cylinder, the unsteady sectional force coefficient decreases.

53

To construct a broader view of the interaction problem, let us review some of our observations. As swirl is added to the flow, the translational effects on the axial sectional force coefficient are not nearly as significant. Particularly, near the vortex, the effects of translation on axial sectional force coefficient become minimal. On the other hand, the same is not true for the side force, and the drag coefficients. Near the vortex, the translational effects significantly alter the direction and magnitude of the forces perpendicular to the axis of the cylinder. These observations strengthen the arguments made earlier that translation alters the circulation around the cylinder, giving rise to an unsteady side force. An unsteady side force could account for the significant changes in the sectional force coefficients in the horizontal plane while leaving the axial force relatively unaffected.

From an engineering design standpoint, we will assess the significance of the translational effects by considering the ratio of the magnitude of the unsteady forces to the steady forces, figure 14. This figure shows that the horizontal sectional force coefficients are increased significantly as the model approaches the vortex. However, after the model has passed through the vortex region, and it is sufficiently far from the vortex, translation causes a significant reduction in the horizontal sectional force coefficients. Figure 15b also reveals that the axial sectional force coefficient increases as a result of the motion of the model toward the vortex. However, as the model is situated well within the updraft region, the effects are minimal. Shortly after the passage of the model through the vortex, the unsteady

54

results show a significant increase over the steady axial sectional force coefficients. Further away as the model continues to recede from the vortex, the effects of the translation are rather unimportant, and eventually, the unsteady axial sectional force coefficient becomes smaller than the corresponding steady sectional force coefficient.

CHAPTER IV

THEORETICAL CONSIDERATIONS

4.1 Introductory Remarks

In this chapter, we survey some of the previous work in this area,
and examine some new ideas. Our goal is not to offer an accurate model
from a quantitative standpoint. It should be clear by now that the
tremendous complexity of the problem places a quantitavely accurate
model beyond the state of the art. Thus, the nature of our analysis is
primarily quantitative, and our efforts shall be focused on under-
standing the problem as opposed to making quantitative predictions.

4.2 Literature Survey

A method for the calculation of tornadic wind loads on structures
has been suggested by Wen (29). In his analysis, Wen decomposes the
total force on the structure into two components: drag and inertia
forces. The drag force is assumed to be proportional to the square of
velocity, and the inertia force is assumed to be proportional to the
fluid acceleration. The idea is not new. In fact, Stokes (35) first
suggested such an approach to explain the motion of a pendulum in a
viscous fluid. Wen's semi-empirical equation may be written in the
following form:

$$R(t) = \frac{1}{2} \rho C_D DU|U| + \frac{\pi}{4} \rho C_m D^2 \frac{dU}{dt} \tag{8}$$

$R(t)$ is the total force per unit length, U is the local fluid velocity, D is the characteristic length scale of the structure, and C_D and C_m are constants of proportionality, which are determined experimentally. U and $\frac{dU}{dt}$ are calculated from a flow model proposed by Kuo (30). Basically, Wen's approach is to find the best fit, by adjusting C_D and C_m, of a curve, furnished by Kuo's expressions for U and $\frac{dU}{dt}$. Wen's approach has been criticized on the basis that it does not properly represent the acceleration term in a flow having a strong velocity gradient. Theoretical arguments by Hunt (32,33) for flows having large velocity gradients, have shown the inadequacy of Wen's way of calculating the acceleration term. Apart from Hunt's work, experimental observations of Vickery (34) demonstrate the limitations of the application of Wen's approach, in turbulent flows. Furthermore, as the structure enters the core region, Wen's idea fails completely. Hunt (31) has suggested an alternative approach using an inviscid, irrotational flow model. The argument to justify such a potential flow model is based on the studies by Keulegan and Carpenter (35). In their experiments, Keulegan and Carpenter measured forces on cylinders and flat plates in oscillating fluids. Their final conclusion was that if the ratio of the length scale of the flow to the length scale of the structure is less than 10, then the wake behind the object shrinks, and the drag coefficient approaches a numerical value of about 5. The length scale of the flow is calculated by taking the product of the maximum velocity and the period of oscillation. It turns out that Keulegan and Carpenter's results are consistent with the application of the

57

potential flow theory to the oscillating cylinder in a stationary fluid problem.

Hunt has extended Keulegan and Carpenter's conclusions to the tornado-structure interaction problem. Hunt has argued that if the analog of Keulegan and Carpenter's so call "period parameter" has a value of approximately 10, then the potential flow model becomes a reasonable approximation. Throughout our experiments, many observations have been made that are inconsistent with potential flow theory. There appears to be a contradiction between Hunt's ideas concerning the tornado-structure interaction and the present experiments. For this reason, we will consider a potential flow model to assess its utility in explaining our observations.

4.3 An Approximate Solution Using a Potential Flow Model

In order to make the flow calculations possible, we consider an infinitely long circular cylinder in a vortex-sink flow. The vortex-sink combination is a reasonable assumption for the flow outside of the core region. Inside the core radius, the flow behaves much like a rigid body rotation. The potential flow model is a tempting idea, because its application to the flow enables one to calculate the entire flow field.

The fundamental physical ideas, as well as the notation, are those of Ashley and Landahl (36). The expression for the complex potential due to a sigularity of strength Q located at a distance z_0 from the origin, with a circular cylinder of radius a at the origin, in the complex z plane, is given by,

$$W = \phi + i\psi$$

$$W = A \ln(Z - Z_0) + Q^* \ln\left(\frac{a^2}{Z} - Z_0^*\right) \tag{9}$$

where the superscript ( )* denotes the complex conjugate. Here Q is

equal to $\frac{\Gamma}{2\pi} + i\frac{q}{2\pi}$, where Γ is the circulation and q is the

volumetric flow rate per unit area for the sink. The components of

force are related to the complex potential by the unsteady Blausius

equation

$$dF_x - idF_y = i\frac{\rho}{2}\frac{dW}{dZ}dW^* + i\rho\frac{\partial\phi}{\partial t}dZ^* \tag{10}$$

where

$$\frac{\partial\phi}{\partial t} = R_e\left\{\frac{\partial W(Z)}{\partial t}\right\} \tag{11}$$

and

$$\frac{\partial\phi}{\partial t} = \frac{\partial W^*}{\partial t} + i\frac{d\psi_B}{dt} \tag{12}$$

where ϕ and ψ are the real and imaginary parts of W, respectively.

Equation (9) may be integrated along the contour C_B, which is the
surface of the cylinder. Noting that the integral of the quantity $\frac{d\psi_B}{dt}$
around the contour C_B must vanish, we obtain

$$F_x - iF_y = 2\pi\rho\frac{a^2 Z_0^*}{z_0 z_0^* - a^2}V_0^2 - 2\pi\rho\frac{a^2 Z_0^*}{r_0^2}V_0 e^{-i\phi}\frac{dZ_0}{dt} \tag{13}$$

where V_0 is the magnitude of the velocity due to the vortex-sink com-

bination, at a distance r_0 from the singularity, and r_0 is the radial

distance of the singularity from the center of the cylinder. Here, ϕ

is the imposed swirl angle. The first term of the right hand side of

the equation (13), gives the steady contribution, and the second term

59

gives the unsteady contribution of the forces. Since $z_0 = x_0 + iy_0$, we obtain

$$(F_x - iF_y)_{steady} = \frac{2\pi\rho \ a^2 \ r_0 \ V_0^2}{r_0^2 - a^2} \ e^{-i \ \tan^{-1} \ (\frac{y_0}{x_0})} \qquad (18)$$

For the unsteady component of the force, suppose that the singularity undergoes translation parallel to the x-axis. Then, the expression for z_0 is

$$x_0 = V_{tr} \ t$$
$$z_0 = V_{tr} \ t + iy_0 \qquad (15)$$

Here V_{tr} is the translational velocity of the singularity relative to the cylinder and it is assumed to have a constant value in the x-direction, that is

$$V_{tr} = \frac{dx}{dt} = constant \qquad (16)$$

The unsteady component of force may be written as,

$$(F_x - iF_y)_{unsteady} = \frac{2\pi\rho \ a \ ^2V_0 \ V_{tr}}{(V_{tr}^2 \ t^2 + y_0^2)^{1/2}} \ e^{-i(\pi \ + \ \tan^{-1} \ (\frac{y_0}{V_{tr}t}) \ + \ \phi)} \qquad (17)$$

Using the appropriate reference quantities, we may now express the potential flow force coefficients as

$$(C_{Fx} - iC_{Fy})_{steady} = \frac{2\pi a \ r_0}{r_0^2 - a_0^2} \ (\frac{V_0}{V_{ref}})^2 \ e^{-i \ \tan^{-1} \ (\frac{y_0}{x_0})} \qquad (18)$$

$$(C_{Fx} - iC_{Fy})_{unsteady} =$$

$$\frac{2\pi a}{(V_{tr}^2 \ t^2 + y_0^2)^{1/2}} \ (\frac{V_0 \ V_{tr}}{V_{ref}^2}) \ e^{-i(\pi \ + \ \tan^{-1} \ (\frac{y_0}{V_{tr} \ t}) \ + \ \phi)} \qquad (19)$$

$$C_{f_{unsteady}} = C_{f_{steady}} + C_{f_{unsteady}} \ due \ to \ translation \qquad (20)$$

A comparison between the potential flow results and the experimental results shows very little argreement. The potential flow model requires two assumptions: two-dimensionality and the absence of vorticity in the flow. The velocity profile at the screen shows significant variations of the radial component of velocity in the vertical direction. Furthermore, in the convection zone, the vertical component of velocity becomes very significant. The flow over the roof section affects the flow around the cylinder significantly. Therefore, two dimensionality is not a sound assumption. The other assumption, irrotationality, is not a particularly good assumption, either. The sheared velocity profile at the screen, and the wake behind the cylinder both generate vorticity. Near the core region, the axial component of vorticity gets very large. Therfore, in this region, it is not reasonable to assume irrotationality.

Our investigations lead to the conclusion that the potential flow theory is not capable of adequately describing the flow and its predictions are not consistent with laboratory observations. A more general conclusion is that Keulegan and Carpenter's criterion of irrotationality should not be generalized to nonperiodic flows.

4.4 Rotational Flow Model

Let us reconsider our assumptions regarding the flow model. Instead of the potential flow, a more complex model must be used. In this section, a three-dimensional, rotational, inviscid model is considered. What follows is purely qualitative, and is intended to evaluate the possibility of the application of such a model.

61

Let us consider an axisymmetric rotational flow of an inviscid

fluid. Taking the curl of the momentum equation, we may write the

vorticity transport equation as

$$\frac{\partial \vec{\omega}}{\partial t} = \nabla \times (\vec{u} \times \vec{\omega}) \tag{21}$$

$\vec{u}$ and $\vec{\omega}$ are velocity and vorticity vectors, respectively. Assuming

that the flow is steady and axisymmetric, we may expand the right hand

side of the equation (21) to obtain

$$\nabla_X (\vec{u} \times \vec{\omega}) = 0$$

$$\frac{\partial}{\partial z} (u\zeta - \xi w) = 0 \tag{22a}$$

$$\frac{\partial}{\partial r} (u\zeta - \xi w) + \frac{(u\zeta - \xi w)}{r} = 0 \tag{22b}$$

$$\frac{\partial}{\partial r} (u\eta - \xi v) - \frac{\partial}{\partial z} (v\zeta - \eta w) = 0 \tag{22c}$$

where $\vec{r} = (r,\theta,z)$, $\vec{u} = (u,v,w)$, and $\vec{\omega} = (\xi,\eta,\zeta)$.

Equations (22a) and (22b) may be used to arrive at the following

conserved quantity:

$$\frac{u\zeta - \xi w}{r} = \text{constant} \tag{23}$$

Equation (22c) may be written in an alternative way;

$$\eta \left(\frac{\partial u}{\partial r} + \frac{\partial w}{\partial z} \right) + u \frac{\partial \eta}{\partial r} + w \frac{\partial \eta}{\partial z} = v \left(\frac{\partial \xi}{\partial r} + \frac{\partial \zeta}{\partial z} \right) + \xi \frac{\partial v}{\partial r} + \zeta \frac{\partial v}{\partial z}$$

$$\eta \left(\nabla \cdot \vec{u} - \frac{u}{r} \right) + \vec{u} \cdot \nabla \eta = v \left(\nabla \cdot \vec{\omega} - \frac{\xi}{r} \right) + \vec{\omega} \cdot \nabla v$$

But $\nabla \cdot \vec{u} = 0$ by continuity. And

$$\nabla \times (\vec{u} \times \vec{\omega}) = (\nabla \cdot \vec{u})\vec{\omega} + (\nabla \cdot \vec{\omega})\vec{u} = 0$$

Since $\vec{u} \neq 0$, then

$$\nabla \cdot \vec{\omega} = 0$$

62

Thus we have

$$\vec{u} \cdot \nabla \eta - \frac{u\eta}{r} = \vec{\omega} \cdot \nabla v - \frac{v\zeta}{r} \tag{24}$$

Equations (23) and (24) may be used to arrive at some conclusions about the vorticity distribution in the flow. Note that the trivial solution of $\vec{\omega} = 0$ is in fact the potential flow solution. Therefore, we will consider the nontrivial case of $\vec{\omega} \neq 0$.

In the convergence zone, w is small due to the fact that it must vanish at $z = 0$, and $z = h$, where h is the height of the inflow layer. Therefore, $\frac{u\zeta}{r}$ should not change significantly throughout the convergence zone. Since u decreases with increasing distance, then axial vorticity, ζ, must increase with increasing distance. In particular, if we consider the approximation that $u \propto \frac{1}{r}$, then $\zeta \propto r^2$. As we enter the convection zone, w is no longer small compared to u. Therefore, axial vorticity may take on a different functional form to satisfy equation (23).

During our discussion of the pressure distribution, we noticed certain similarities between our results and those obtained from the slow motion of a cylinder in a rigidly rotating flow, in which ζ has a constant value. Thus, if we allow for axial vorticity to have a non-zero value in the convergence zone, then for small displacements, $\zeta \propto r^2$ does not change significantly. It may be possible to argue that the flow at a radial distance r_0 enjoys certain similarities to a rigidly rotating flow having the same axial vorticity.

Next, let us consider equation (24). The interesting feature of this equation is its symmetry. In fact, if $\vec{u}$ and $\vec{\omega}$ have the same

63

functional dependence on r and z, then (24) is satisfied. Recalling
that in the convergence zone $u \propto r^{-1}$, and $\zeta \propto r^2$, we may use the
symmetry of equation (24) to argue that in this region $\xi \propto r^{-1}$, and
$w \propto r^2$.

The addition of an obstacle to the flow is essentially adding a
vorticity production mechanism to the flow. As the flow separates and
forms a wake behind the object, vorticity is shed into the flow. The
additional vorticity is then convected through the flow according to
the convection mechanisms which were discussed. The production of
vorticity for a moving object would depend on the characteristic
length scale of the object, and the translational velocity. Using the
characteristic values of velocity and length scale, it is possible to
form a vorticity production time scale:

$$\frac{\partial}{\partial t} \omega_p = \frac{\partial}{\partial t} (\nabla \times v)$$

which we may nondimensionalize by

$$t' = \frac{t}{\tau_p} \quad , \quad \nabla' = L \nabla \quad , \quad V' = \frac{V}{V_{tr}}$$

where the primed variables are nondimensional.

$$\tau_p = \frac{L}{V_{tr}} \frac{\frac{\partial}{\partial t'} \omega'_p}{\frac{\partial}{\partial t'} (\nabla' \times V')}$$

Therefore:

$$\tau_p = \frac{L}{V_{tr}} \tag{25}$$

where L is the characteristic length scale of the model, and V_{tr} is the
translational velocity. We may also define a vorticity convection time

64

scale using the local undisturbed fluid velocity, and some character-
istic length scale of the flow. r_c, the core radius, may be used as a
characteristic length scale of flow, because it is the distance over
which important dynamical changes occur in the flow. Therefore, in a
similar way, as our vorticity convection time scale we obtain

$$\tau_c = \frac{r_c}{V} \tag{26}$$

where V is the undisturbed local fluid velocity. The rate at which
vorticity is produced scales with $\frac{1}{\tau_p}$, and the rate at which it is
convected scales with $\frac{1}{\tau_c}$. Therefore, if $\tau_p \ll \tau_c$, then vorticity is
produced at a faster rate than it is convected. In this case, the
translational effects should dominate the flow. On the other hand, if
$\tau_c \ll \tau_p$, then the convection of vorticity dominates the production
of vorticity. This is to say that the produced vorticity does not
alter the flow significantly, since it is quickly "washed" out of the
flow. In this case, it is not expected to see any significant effects
as a result of the translation. Aside from the two limiting cases, if
$\tau_c \approx \tau_p$ then the production of vorticity and the convection of vortic-
ity both contribute to the flow. This is to say that vorticity is pro-
duced at a significant rate, but it is not quickly convected down-
stream. Therefore, the additional vorticity is capable of affecting
the local flow which in turn interacts with the wake behind the object.
The result is a highly complex interaction between the translating
object and the flow. In this case, one cannot add the effects of the
flow around the structure (steady effects), and the effects of a pure
translation (essentially a drag force) to calculate the total effect.

65

Since the diameter of the cylinder, taken as the model length scale, and r_c are of the same order of magnitude, the comparison between τ_c and τ_p is essentially a comparison between the translational velocity and the local undisturbed fluid velocity. In our experiments, when the model is at its largest distance from the core, the velocities are roughly of the same order of magnitude. As the model approaches the core, the undisturbed velocity increases, giving rise to the expectation that the effects of translation should become less noticable. For the most part, the translational velocity and the undisturbed fluid velocity maintain the same order of magnitude, resulting in a highly complex interaction. These arguments and our measurements do not disagree.

CHAPTER V

SUMMARY, CONCLUSIONS, AND RECOMMENDATIONS FOR FUTURE RESEARCH

The results of this experiment indicate that the unsteady tornado-structure interaction produces significantly different results than the steady interaction. The contribution due to the translational effects cannot be accounted for by a simple addition of a drag force.

Translation produces a more symmetric distribution of the pressure around the cylinder, while causing a more significant pressure drop, and therefore, making failure of the structure due to "bursting" a stronger likelihood. The increase in the horizontal sectional force coefficients due to the translation of the model may result in failure in the "blown over" mode. An examination of the sectional force coefficients over the dome section of the model reveals very strong axial force coefficients. A strong force acting on the dome may cause a localized failure which could propagate throughout the structure, and cause the total failure of the structure.

The effects of translation on the horizontal sectional force coefficients are far more pronounced than the translational effects on the axial force coefficients. Therefore, it is believed that the translation causes significant changes in the circulation around the

67

cylinder. It is possible to account for the changes in the circulation around the cylinder by an unsteady sideforce.

The enormous complexity of the flow does not allow for analytical calculations using relatively simple models, such as a two-dimensional potential flow model. Quantitative calculations require far more sophisticated models and analytical techniques.

It is found that the motion of the cylinder causes significant changes in the background flow field.

Digital storage of the signal and on line data processing can easily make it possible to study a greater variety of situations over a much wider range of swirl ratios, and translational speeds, with significantly improved precision. Such improvements would also make it possible to collect data at many more locations on the model, for improved accuracy in the calculation of the force coefficients. More sophisticated measurement techniques, such as laser velocimetery, can also give a significant improvement in the accuracy of the results.

Development of a flow visualization technique, capable of visualizing the unsteady interaction phenomenon can be extremely helpful in the interpretation of the results.

Since the interaction has a significant effect on the background flow, it may not be justifiable to translate the model relative to the vortex, to model the interaction phenomenon. One must search for a way of translating the vortex, relative to a stationary model.

The cylinder-hemisphere combination, used as the model, adds considerable difficulty to an already complex flow problem. It may prove helpful to study this problem with a much simpler model, such as a two

dimensional (large length of diameter ratio) cylinder, or a sphere. In fact, it may be helpful to, initially, study the translation of a vortex without the presence of any obstacles to enhance one's understanding of the background flow, and then, study the dynamic vortex-structure interactions.

REFERENCES

1. Davies-Jones, R; and Kessler, E. (1974), "Tornadoes", Weather and Climate Modification, edited by W.N. Hess, pp. 552-595, Wiley.

2. Mehta, K.C., "Windspeed Estimates: Engineering Analysis", Proceedings of the Symposium on Tornadoes, Lubbock, Texas, 1976.

3. Davenport, A.G., 1963; Paper 2, Syn. No. 16, Wind effects on building and structures. National Physics Lab. England.

4. Jensen, M. and Frank, N., 1965; Danish Tech. Press, Copenhagen.

5. Jensen, M., 1958; Ingenioren, Int. Ed. 2.

6. Cermak, J.E., Sadeh, W.Z., and Hsi, G., 1970; National Bureau of Standards, Bldg. Sci. Series No. 30, pp. 45-59.

7. Marshall, R.C. and Thom, H.C.S (editors), 1970; National Bureau of Standards, Bldg. Sci. Series, No. 30.

8. Parmelee, R.A., (editor), 1970; Proc. of Design Sym., Northwestern University, March 23.

9. Chang, C.C., "Tornado Wind Effects on Buildings and Structures with Laboratory Simulation", Third International Conference on Wind Effects on Buildings and Structures, Tokyo, Japan, 1971.

10. Jischke, M.C. and Light, B.D., "Laboratory Simulation of Steady Tornadic Wind Loads on Structures", Research Report OU-AMNE-79-12, School of Aerospace, Mechanical, and Nuclear Engineering, University of Oklahoma, 1979, p. 108.

11. Mehta, K.C., Minor, J.E., and McDonald, J.R., "The Tornadoes of April 3-4, 1974; Windspeed Analysis", ASCE National Structural Engineering Conference, New Orleans, Louisiana, 1975.

12. McDonald, J.R., :The Hereford Tornado of April 19, 1971", Institute of Disaster Research Report, Texas Tech. University, Lubbock, Texas, 1971.

13. Kessler, E. "Tornadoes: State of Knowledge", ASCE Proceedings: Structural Division, Vol. 104, February, 1978, pp. 352-357.

14. Hoecker, W.H., "Windspeed Airflow Patterns in the Dallas Tornado of April 2, 1957", Monthly Weather Review, Vol. 88, pp. 167-180, 1960.

15. Hoecker, W.H., "Three-Dimensional Pressure Pattern of the Dallas Tornado and Some Resultant Implications", Monthly Weather Review, Vol. 89, pp. 533-542, 1961.

16. Goldman, J.L., "The Illinois Tornadoes of 17 and 22 April 1963", SMRP Research Paper No. 39, University of Chicago, Chicago, Illinois, 1965.

17. Monji, N., :Laboratory Studies of Tornado Vortices", Cooperative Institute of Mesoscale Meteorology Studies Report No. 2, Norman, OK, Sept. 1980.

18. Ward, N.B., "The Exploration of Certain Features of Tornado Dynamics Using a Laboratory Model", J. Atom. Sci., Vol. 29, No. 6, Sept., 1972, pp. 1194-1204.

19. Ward, N.B., "The Newton, Kansas Tornado Cyclone of May 24, 1964", Reprints Eleventh Radar Conf., Boulder, CO, Amer. Meteor. Soc., 1964, pp. 410-415.

20. Jischke, M.C. and Parang, M., "Fluid Dynamics of a Tornado-Like Vortex Flow", University of Oklahoma AMNE Report, 1975.

21. Jischke, M.C. and Parang, M., "Properties of Simulated Tornado-Like Vortices", J. Atmospheric Sciences, Vol. 31, 1974, pp. 506-512.

22. Church, C.K., Snow, J.T., and Agee, E.M., "Tornado Vortex Simulation at Purdue University", Bulletin of the American Meterological Society, Vol. 58, 1977, pp. 900-908.

23. Greenspan, H.P., The Theory of Rotating Fluids, Cambridge University Press, 1980.

24. Davies-Jones, R.P., "The Dependence of Core Radius on Swirl Ratio in a Tornado Simulator", J. Atmospheric Sciences, Vol. 30, 1973, pp. 1427-1430.

25. Cermak, J.E., "Aerodynamics of Buildings", Annual Reviews of Fluid Mechanics", Vol. 8, 1976, pp. 75-106.

26. Cockrell, D.J. and Lee, B.E., "Production of Sheared Profiles in a Wind Tunnel by Cylindrical Rods Placed Normal to the Stream", J. Royal Aeronautical Society, Vol. 80, 1966, pp. 724-725.

27. Light, B.D. "Laboratory Simulation of Tornadic Wind Loads on Structures", Master's Thesis, University of Oklahoma, 1980.

28. Leslie, F.W., "Dynamic Behavior of Single and Multiple Vortex Tornadoes Inferred from Laboratory Simulation", Ph.D. Dissertation, University of Oklahoma, 1979.

29. Wen, Yi-Kwer, "Dynamic Tornadic Wind Loads on Tall Buildings", Journal of the Structural Division, Proceedings of the American Society of Civil Engineers, Vol. 101, No. ST 1, January 1975. pp. 169-185.

30. Kuo, H.L., "Axisymmetric Flows in the Boundary Layer of a Maintained Vortex", Journal of Atmospheric Sciences, Vol. 28, No. 1, January 1971, pp. 20-41.

31. Hunt, J.C.R., Discussion on "Dynamic Tornadic Wind Loads on Tall Buildings", Journal of the Structural Division, Proceedings of the ASCE, Vol. 101, No. St. 11, November 1975, pp. 2446-2449.

32. Hunt, J.C.R., "A Theory of Turbulent Flow Around Two-Dimensional Bluff Bodies", Journal of Fluid Mechanics, Vol. 61, 1973, p. 625.

33. Hunt, J.C.R., "A Theory of Fluctuating Pressures of Bluff Bodies in Turbulent Flows", International Union of Theoretical and Applied Mechanics-International Association of Hydraulics Research Symposium on Flow Induced Structural Vibration, Karslruke, Germany, 1972.

34. Vickory, B.J. and Kao, K.J., "Drag or Along-Wind Response of Slender Structures", Journal of the Structural Division, ASCE, Vol. 98, No. St. 1, Proc. Parer 8635, January 1972, pp. 21-36.

35. Keulegan, G.H. and Carpenter, L.H., "Forces on Cylinders and Plates in an Oscillating Fluid", Journal of Research, National Bureau of Standards, Vol. 60, No. 5, May 1958, pp. 423-440.

36. Ashley, H. and Landahl, M., Aerodynamics of Wings and Bodies, Addison-Wesley Publishing Co., Inc., 1965.

37. Golstein, S. (editor) Modern Developments in Fluid Dynamics, Dover, 1965.

38. Schlichting, H., Boundary Layer Theory, 7th ed., McGraw-Hill, 1979.

4. TITLE AND SUBTITLE *(Add Volume No., if appropriate)*

EXPERIMENTAL INVESTIGATION OF UNSTEADY TORNADIC WIND LOADS ON STRUCTURES

2. *(Leave blank)*

3. RECIPIENT'S ACCESSION NO.

7. AUTHOR(S)

Martin C. Jischke and Farid Moslehi

5. DATE REPORT COMPLETED

MONTH	YEAR
April	1984

9. PERFORMING ORGANIZATION NAME AND MAILING ADDRESS *(Include Zip Code)*

School of Aerospace, Mechanical & Nuclear Engineering
University of Oklahoma
865 ASP Avenue
Norman, OK   73069

DATE REPORT ISSUED

MONTH	YEAR
June	1984

6. *(Leave blank)*

8. *(Leave blank)*

12. SPONSORING ORGANIZATION NAME AND MAILING ADDRESS *(Include Zip Code)*

Division of Radiation Programs & Earth Sciences
Office of Nuclear Regulatory Research
U.S. Nuclear Regulatory Commission
Washington, D. C.   20555

10. PROJECT/TASK/WORK UNIT NO.

11. FIN NO.

B6241

13. TYPE OF REPORT

TECHNICAL

PERIOD COVERED *(Inclusive dates)*

15. SUPPLEMENTARY NOTES

14. *(Leave blank)*

16. ABSTRACT *(200 words or less)*   Ward's tornado simulator was used to model the effects of a tornado-like vortex on a cylindrical model structure. The experiment was conducted at swirl angles of 0° and 45°. Pressure coefficients were measured at different locations on the model for steady and unsteady cases, corresponding to situations where the relative velocity between the vortex and model is zero and nonzero. Results are presented in the forms of sectional pressure coefficient profiles, and sectional force coefficients. Pressure profiles show that there are significant differences between the steady and unsteady results. Translation of the model through the simulator produces a more symmetric pressure distribution, and also results in a more substantial pressure drop on the model.
It is observed that in a flow with swirl angle at 45°, translation causes a significant increase in the horizontal sectional force coefficient. Outside of the core region, translation causes an increase in the axial sectional force coefficient. The formation of very low pressure regions over the top section of the structure leads to very strong axial force coefficients. This may cause the failure to first appear on the roof, and then propagate throughout the structure and cause total failure.

17. KEY WORDS AND DOCUMENT ANALYSIS

17a. DESCRIPTORS

17b. IDENTIFIERS/OPEN-ENDED TERMS

18. AVAILABILITY STATEMENT	19. SECURITY CLASS *(This report)*	21. NO. OF PAGES
Unlimited	Unclassified	
	20. SECURITY CLASS *(This page)* Unclassified	22. PRICE S

NRC FORM 335 (11-81)

UNITED STATES
NUCLEAR REGULATORY COMMISSION
WASHINGTON, D.C. 20555

———

OFFICIAL BUSINESS
PENALTY FOR PRIVATE USE, $300

120555078877   1 1ANIRB
US NRC
ADM-DIV OF TIDC
POLICY & PUB MGT BR-PDR NUREG
W-501
WASHINGTON   DC 20555

EXPERIMENTAL INVESTIGATION OF UNSTEADY TORNADIC WIND LOADS ON STRUCTURES